MASTER OF SCIENCE THESIS

Exploration of Non-MPB PZT Compositions for High Piezoelectric Voltage Sensitive 0-3 Composites

AMAL SHAJI KARAPUZHA

FACULTY OF AEROSPACE ENGINEERING

Delft University of Technology

2014

TU Delft Delft University of Technology

Exploration of Non-MPB PZT Compositions for High Piezoelectric Voltage Sensitive 0-3 Composites

Master of Science Thesis

For obtaining the degree of Master of Science in Aerospace Engineering
at
Delft University of Technology

Amal Shaji Karapuzha

17th December 2014

Faculty of Aerospace Engineering

Delft University of Technology

DELFT UNIVERSITY OF TECHNOLOGY

FACULTY OF AEROSPACE ENGINEERING

DEPARTMENT OF AEROSPACE STRUCTURES AND MATERIALS

NOVEL AEROSPACE MATERIALS GROUP

GRADUATION COMMITTEE

Dated: 17th December 2014

Committee chairman:

Prof. dr. W.A. Groen

Committee members:

Prof. dr. ir. S. van der Zwaag

Dr. ir. W G. Sloof

N K. James M.Sc.

Abstract

Piezoelectric composites provide an opportunity to make robust piezoelectric sensors. These materials are based on piezoelectric ceramic powders or particles, which are dispersed in a polymer matrix. In most cases, piezoelectric composites use the same ceramic compositions as the ones used in piezoelectric ceramics. These compositions consist of lead zirconium titanate (PZT) with a composition close to the morphotropic phase boundary (MPB). This research work focuses on exploring the performance of non-MPB compositions of PZT ceramic particles in order to obtain high voltage sensitive 0-3 PZT-Epoxy composites.

The PZT ceramic compositions ($PbNb_{0.01}[Zr_xTi_{(1-x)}]O_3$), ranging from pure tetragonal lead titanate (x=0) to rhombohedral (x=0.80) were prepared using the mixed oxide method. These ceramic particles were characterized using XRD, SEM and particle size analyser and were used to prepare both sintered ceramics and 0-3 PZT-epoxy composites. The effect of the ceramic filler composition on the dielectric and piezoelectric properties of the PZT-Epoxy composites was investigated. Unlike PZT ceramics, the best piezoelectric properties were not observed in the MPB-based composites but in the pure tetragonal phase. It was observed that the dielectric constant of the ceramic particles had minimal influence on the effective dielectric constant (ε_r) and the piezoelectric charge constant (d_{33}) of the piezoelectric composite due to the depolarization effect of the high dielectric filler materials. The experimentally determined values of the dielectric and piezoelectric properties of the piezoelectric composites were validated using analytical models. The influence of electric fatigue on the polarization of the $PbTiO_3$ (PT) and morphotropic phase boundary (MPB) based composites were also examined.

Finally, a material selection criterion was proposed in order to develop piezoelectric composites with high voltage sensitivity. This general material selection criterion is not limited to PZT based ceramics but is also applicable to lead-free ceramic filler materials. Thus, the current research work paves the way for the development of environmental friendly lead-free piezoelectric composites devices with enhanced sensory properties.

Acknowledgement

It gives me immense pleasure to express my sincere gratitude to my principal supervisor Prof. dr. Pim Groen for providing me with the opportunity to work on piezoelectric composite materials under the Smart Materials team of the Novel Aerospace Materials Group (NovAM). He was always a continuous source of guidance, inspiration, and motivation. It was his lectures which motivated me to concentrate my graduate research on piezoelectric composites.

I would also like to thank my second supervisor, Prof. dr. ir. Sybrand van der Zwaag, whose valuable suggestions and guidance during the progress meetings proved to be an important source of inspiration and motivation throughout the thesis. I would also like to thank Dr. ir. Wim G. Sloof for being on my thesis defence committee and for his valuable time and consideration.

I am extremely thankful to my daily supervisor Nijesh K. James, who spent endless hours in helping me out right from the start of this research work, in spite of his busy schedule. His valuable comments and suggestions played a major role in elevating the quality of this thesis to its present elegant form. The research skills and knowledge I have gained from him will benefit me greatly in my future endeavours.

I would also like to take this opportunity to thank Daniella Deutz, Hamideh Khanbareh and Jibran Khaliq for providing me with all kinds of possible help, advice and feedback during the course of this work. I also would like to thank other members of the NovAM Group for making my tenure with the group an unforgettable experience. I also would like to thank Mrs. Shanta Visser for helping me with all the administrative works related to my thesis work.

Finally, I would like to thank my parents and sister, who have provided continuous support and encouragement to follow my dreams, even if that involved moving to the other side of the world. They have been there to help me through all the challenges along the way and I certainly wouldn't have made it this far without them.

Table of Contents

List of Figures

List of Tables

Glossary

Abbreviations

Ba	Barium
BNT	Bismuth Sodium Titanate
BT	Barium Titanate
DEP	Dielectrophoresis
MPB	Morphotropic Phase Boundary
Nb	Niobium
Pb	Lead
PT	Lead Titanate ($PbTiO_3$)
PVA	Polyvinyl alcohol
PVDF	Polyvinylidene fluoride
PZT	Lead zirconate titanate ($Pb[Zr_xTi_{(1-x)}]O_3$)
RT	Room Temperature
SEM	Scanning Electron Microscopy
Ti	Titanium
XRD	X-ray Diffraction
Zr	Zirconium

Symbols

α	Depolarization factor
β	Impermitivity component
ε_c	Dielectric constant of composite
ε_f	Dielectric constant of filler
ε_{ij}	Dielectric constant

ε_o	Permittivity of free space
ε_m	Dielectric constant of polymer matrix
θ	Incident X-ray angle
ξ	Permittivity
ρ	Density
σ	Stress
φ	Poling ratio

A	Electroded area
C	Capacitance
D	Electric Displacement
d	Thickness
d_{ij}	Piezoelectric Charge Constant
E	Electric Field
E_c	Coercive Field
g_{ij}	Piezoelectric Voltage Constant
k_{ij}	Piezoelectric Coupling Coefficient
n	Shape Factor
P	Polarization
P_s	Saturated Polarization
P_r	Remnant Polarization
S	Compliance Coefficients
T_c	Curie temperature
V_f	Volume percent of filler material
V_m	Volume percent of matrix material

1. An Overview of Piezoelectric Ceramics and Composites

1.1 Introduction

The term 'piezoelectricity' is derived from an ancient Greek work *piezein*, which means to 'squeeze' or 'press'. The piezoelectric effect was discovered by Pierre Curie and Jacques Curie in 1880, when they observed that crystals of tourmaline, quartz, topaz and Rochelle salt generated electrical polarization, when stressed in particular directions. The amount of charges produced was found to be proportional to the pressure applied and these charges got diminished on withdrawal of the pressure

Piezoelectric materials are considered as an important member of the Smart Materials Age due to its ability to produce electrical energy from mechanical energy. This unique property enables the piezoelectric materials to be for sensing applications such as pressure sensors, force sensors and accelerometers. In addition, these piezoelectric materials can also be used as actuators, during which they respond to an applied voltage, resulting in a mechanical strain and cause the 'smart' structure, in which they are embedded, to undergo deformation. The same technique can also be used to control and suppress vibration. Hence it can be seen, if properly designed, the same piezoelectric material can be used as an actuator or sensor within a structure and thus is expected to be an integral part of the 'smart' systems, which have a variety of potential aerospace applications such as active vibration control, energy harvesting and structural health monitoring.

In this chapter, the general characteristics of piezoelectric materials are reviewed. A brief introduction to the macroscopic and microscopic aspects of piezoelectric materials is provided initially, which confirms the phenomenon of piezoelectricity. Later on, a general review on the constitute equations and coefficients of piezoelectric effect, along with a brief outlook on different types of piezoelectric materials and its applications, are given. The chapter concludes by providing an overview regarding the motivation behind this research work and its main objectives.

1.2 Piezoelectric Effect

The piezoelectric effect is a linear electromechanical interaction between the mechanical and electrical state in crystal without a center of symmetry and is reversible in nature [1]. This piezoelectric behaviour can be classified into two – *direct piezoelectric effect* and *indirect piezoelectric effect*.

1.2.1 Direct Effect

When a mechanical load is applied on a piezoelectric material, electric charges are generated on the surface of the material, resulting in the formation of an electric field. This effect is known as *direct piezoelectric effect* [1] and is shown in Fig. 1.1. This electric field generated can be tapped as electric voltage by the application of electrodes on both sides, which are normal to the direction of the applied mechanical load, of the piezoelectric materials. This mode of application of piezoelectric material enables it to be used for sensory applications such as energy harvesters [2] and pressure sensors [3].

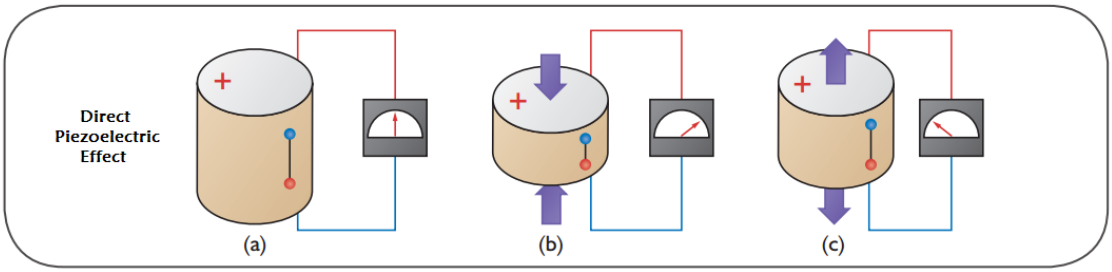

Fig. 1.1: Direct Piezoelectric Effect [4]

1.2.2 Inverse Effect

Converse to the direct piezoelectric effect, when an electric field is applied on a piezoelectric material, it gets deformed. This effect is known as inverse or converse piezoelectric effect and is shown in Fig. 1.2. This mode of piezoelectric effect enables the piezoelectric material to act as actuators and have potential applications in the field of adaptive or morphing structures. In addition, from Fig. 1.2(c) it can be seen that by the application of an AC voltage, it is possible to expand and contact the piezoelectric material alternatively.

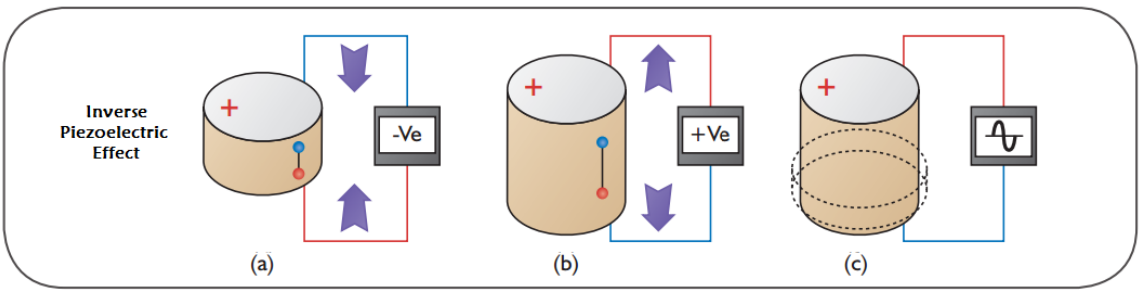

Fig. 1.2: Inverse Piezoelectric Effect [4]

1.2.3 Origin of Piezoelectricity

The origin of piezoelectric effect is attributed towards the asymmetry in the unit cell and the resultant generation of electric dipoles due to the mechanical distortion leading to a net polarization at the crystal surface. Fig. 1.3 shows the typical perovskite crystal structure, for example barium titanate ($BaTiO_3$). Above a critical temperature, known as the *Curie temperature* (T_c), the crystal structure is cubic, as shown in Fig. 1.3(a), with A^{2+} ions at the cube corners, O^{2-} at the face centres and B^{4+} ions at the body centre. Below the *Curie temperature,* the location of the B^{4+} cation does not coincide with the oxygen octahedron, leading to a permanent electric dipole, as shown in Fig. 1.3(b).

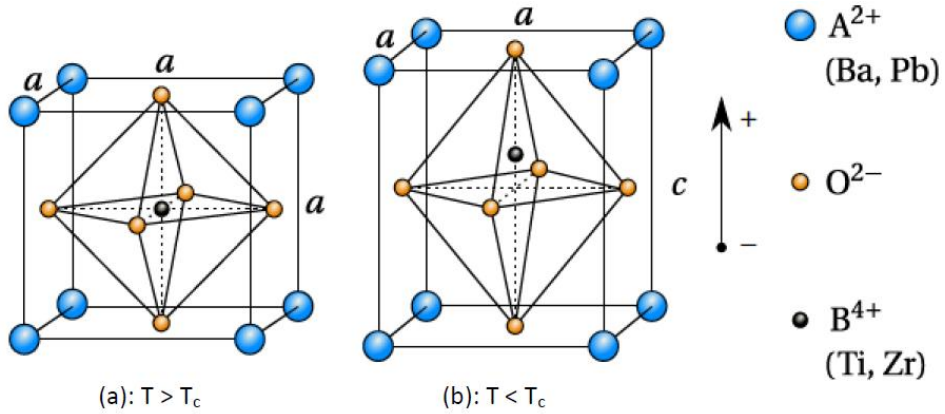

Fig. 1.3: The perovskite crystal structure [5]

Apart from above mentioned single crystal materials, there also exists an important class of piezoelectric materials known as ferroelectric ceramics, which are synthesized by sintering of metal oxides such as the lead zirconate titanate (PZT), bismuth sodium titanate (BNT) and . These ferroelectric ceramics can be considered as a collection of single crystals and globally this type of material do no possess any piezoelectric properties due to the randomly oriented ferroelectric domains within the ceramics before poling, as shown in Fig. 1.4(a) [5].

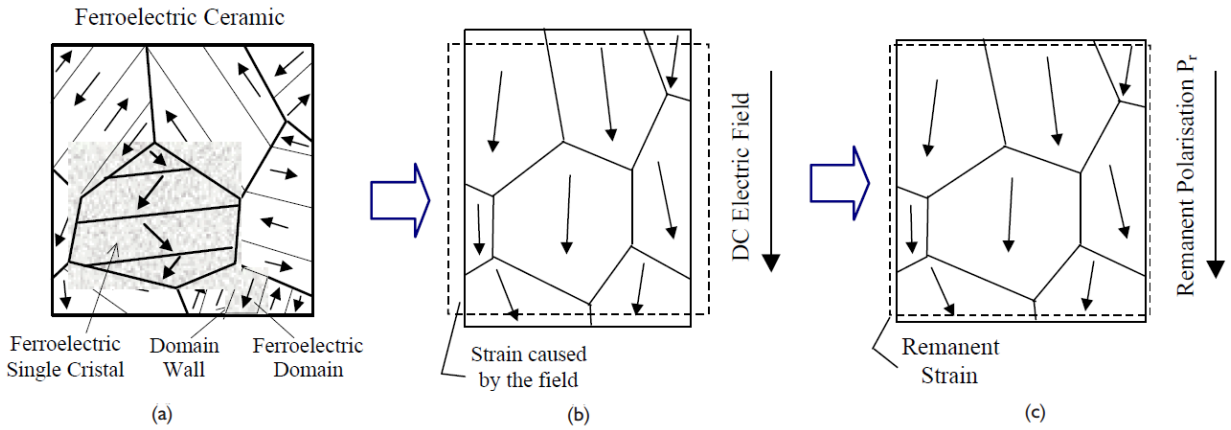

Fig. 1.4: Schematic illustration of the Poling process [6]

During the poling process, a strong external DC electric field is applied on the piezoelectric material in order to reorient the domains in the direction of the applied electric field. But it should be noted that all the domains will not become exactly aligned on the application of the external field and some of the domains gets aligned only partially whereas some do not align at all (Fig. 1.4(b)). The reason behind this can be attributed to the presence of intergranular stresses, which tends to keep the polarity of the domains in their initial position itself, thereby preventing the switching of the domains to it most favourable direction (i.e. direction of applied field). In addition, the crystal imperfections could also account towards the strain within the grain, which in turn also prevents the reorientation of dipoles. After the removal of the electric field, a *remnant polarization* (P_r) and *remnant strain* remains in the material, which results in the piezoelectricity (Fig. 1.4(c)) [1, 7].

1.3 Piezoelectric Constitutive Equations

The constitutive equations describe the piezoelectric effect based on the coupling of the mechanical and electrical behaviour of the piezoelectric material, i.e., total strain in the piezoelectric material is the sum of mechanical strain induced by the mechanical stress and the actuation strain caused by the applied electric voltage. The electromechanical equations for a linear piezoelectric material used for actuator (Eq. 1.1 and 1.2) and sensor (Eq. 1.3 and 1.4) applications can be written as [8, 9]:

$$\in_i = S_{ij}^{E}\sigma_j + \mathrm{d}_{mi}E_m \tag{1.1}$$

$$D_m = \mathrm{d}_{mi}\sigma_i + \xi_{ik}^{\sigma}E_k \tag{1.2}$$

$$\varepsilon_i = S_{ij}^{D}\sigma_j + \mathrm{g}_{mi}D_m \tag{1.3}$$

$$E_i = \mathrm{g}_{mi}\sigma_i + \beta_{ik}^{\sigma}D_k \tag{1.4}$$

where σ is stress vector [N/m^2], ε is strain vector, E is the vector of applied electric field [V/m], ξ is permittivity [F/m], d is the matrix of piezoelectric charge constants [C/N], S is the matrix of compliance coefficients [m^2/N], D is the vector of electric displacement [C/m^2], g is the matrix of piezoelectric voltage constants [V.m/N = m^2/C] and β is the impermitivity component (m/F). In addition, the superscripts D, E and σ represent measurements taken at constant electric displacement, constant electric field and constant stress respectively and the indexes i, j = 1, 2, . . . , 6 and m, k = 1, 2, 3 refer to different directions within the material coordinate systems, as shown in Fig. 1.5.

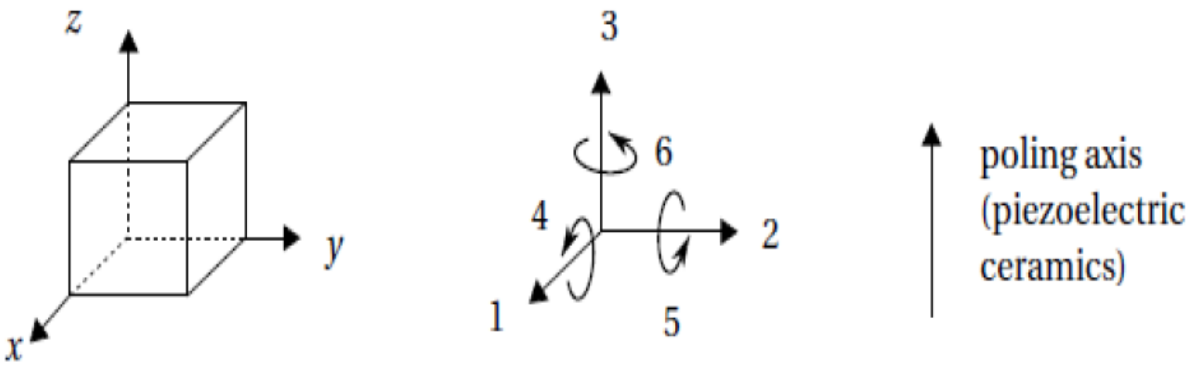

Fig. 1.5: Axis nomenclature[5]

1.4 Piezoelectric Coefficients

The physical meaning of various piezoelectric coefficients – *Dielectric Coefficient (ε_{ij}), Piezoelectric Charge Constant (d_{ij}), Piezoelectric Voltage Constant (g_{ij})* and *Piezoelectric Coupling Coefficients (k)* will be discussed in this section. These coefficients play an important role in the performance of the piezoelectric materials [8, 10, 11].

1.4.1 Dielectric Coefficient (ε_{ij})

Dielectric coefficient (ε_{ij}) determines the charge per unit area in the i-axis due to an electric field applied in the j-axis. The relative dielectric constant (ε_r) of a piezoelectric material with capacitance *C*, thickness *d* and electroded area *A* is given as [12]:

$$\varepsilon_r = \frac{C\ \mathrm{A}}{d\varepsilon_0} \qquad (1.5)$$

where ε_0 is the permittivity of free space = 8.854 x 10^{-12} F/m

1.4.2 Piezoelectric Charge Coefficient (d_{ij})

Piezoelectric charge coefficient is defined as the polarization generated per unit mechanical stress applied to a piezoelectric material (i.e. direct piezoelectric effect) or the mechanical strain experienced by a piezoelectric material per unit of applied electric field (i.e. converse piezoelectric effect) [13]. In case of actuator application, d_{ij} indicates the magnitude of the deformation in the i-direction due to an electric field applied in j-direction (*m/V*) whereas in the case of sensor applications, the subscripts indicate the polarization generated along i-direction due to an applied stress in j-direction. The piezoelectric charge constant is an important role in the pressure sensors, force sensors and actuator applications.

1.4.3 Piezoelectric Voltage Coefficient (g_{ij})

Piezoelectric voltage constant (g_{ij}) is defined as the electric field generated along the j-direction for unit stress applied in i-direction. The piezoelectric voltage coefficient is an important parameter for energy harvesting applications. The relation between ε_{ij}, d_{ij} and g_{ij} is given by Eq. 1.6. From this relation it can be seen that for voltage sensitive application, a piezoelectric material with low ε_{ij} and relatively higher d_{33} is preferred.

$$g_{33} = \frac{d_{33}}{\varepsilon_r \varepsilon_0} \tag{1.6}$$

1.4.4 Piezoelectric Coupling Coefficients (k)

Piezoelectric coupling coefficients represent the ability of a piezoelectric material to transform electrical energy to mechanical energy and vice versa and is given as follows [13]:

$$k^2 = \frac{Stored\ \text{mechanical energy}}{Input\ \text{electrical energy}} = \frac{Stored\ electrical\ energy}{Input\ mechanical\ energy} \tag{1.7}$$

1.5 Piezoelectric Materials

A wide range of natural and man-made materials exhibit the phenomenon of piezoelectric effect and these materials can be as – *single crystal materials* [14, 15], *piezoelectric ceramics* [1], *piezoelectric polymers* [16], *piezoelectric-composites* [11, 17] and *piezoelectric thin films* [18, 19]. Among the various types of piezoelectric materials, piezoelectric ceramics and piezoelectric composites will be explained in detail in the following sections of this chapter.

1.5.1 Piezoelectric Ceramics

Among the various types of piezoelectric ceramics [1], Lead Zirconate Titanate (PZT) based ceramics is the most widely known and used piezoelectric material [20, 21]. PZT has a perovskite structure, as shown in Fig. 1.3. As mentioned in Section 1.2.3, the sintered PZT ceramics lack piezoelectric behaviour on a macroscopic scale due to the random orientation of the domains. Hence it is necessary to pole these PZT ceramics, in order to orient the domains in a particular direction by the application of a strong external electric field (in the order 1 to 4 kV/mm) at an elevated temperature. The dielectric and piezoelectric properties of different types of piezoelectric ceramics have been compiled and tabulated in Table 1.1 below. Since quartz and PVDF are also used as piezoelectric sensors, the dielectric and piezoelectric properties of these materials were also added to the table below.

Table 1.1: Dielectric and piezoelectric properties of ceramics at room temperature

Material	T_c (°C)	ε_r	d_{33} (pC/N)	g_{33}^* (mV.m/N)	Reference
$BaTiO_3$	115	1900	191	11	[1]
$BaTiO_3$-$CaTiO_3$-Co	105	1420	150	12	[22, 23]
$(K_{0.5}Na_{0.5})NbO_3$	420	290	80	31	[24]
KNN-$LiTaO_3$ (5%)	430	570	200	40	[25]
KNN-$SrTiO_3$ (5%)	277	950	200	24	[20]
$LiNbO_3$	1415	29	6	23	[26]
NBT-KBT-LBT	350	1150	216	21	[20]
$PbNb_20_6$	300	225	85	43	[27]
$PbTiO_3$	490	200	50	28	[28]
PLFZT#	548	1266	93	9	[29]
PZT-4	325	1300	289	25	[27]
PZT5A	350	1700	374	25	[27]
PZT-5H	195	3400	593	20	[27]
PZT 507	165	4400	820	21	[30]
PVDF	195	13	-33	-287	[31]
Quartz	573	4.51	2.31	58	[32, 33]

*g_{33} is calculated using Eq. 1.6; KNN: $(K_{0.5}Na_{0.5})NbO_3$; NBT: $(Na_{0.5}Bi_{0.5})TiO_3$; KBT: $(K_{0.5}Bi0.5)TiO_3$; LBT: $(Li_{0.5}Bi_{0.5})TiO_3$; #PLFZT: Fe-doped [(PbLa)(Zr-Ti)O_3]; [26]

The dielectric and piezoelectric properties of PZT ceramics were found to be enhanced in the phase transition region, known as morphotropic phase boundary (MPB), where a significant variation in polarization was observed. This compositionally-induced phase transition of PZT solid solution at a Zr/Ti ratio of 52/48 results in an enhanced dielectric and piezoelectric properties, which is nearly independent over a wide range of temperature [34]. In PZT ceramics, the enhanced properties occurs in the region of the composition-temperature phase diagram where crystal structure changes from tetragonal to rhombohedral via an intermediate monoclinic phase as the Zr/Ti ratio becomes close to 52/48 (see Fig. 1.6) [1, 35]. The significance of this MPB is so intense that search for new piezoelectric materials (such as lead-free [34] and piezoelectric composites [11]) are naturally focused on those exhibiting similar MPB transition, expecting dominant dielectric and piezoelectric properties [36].

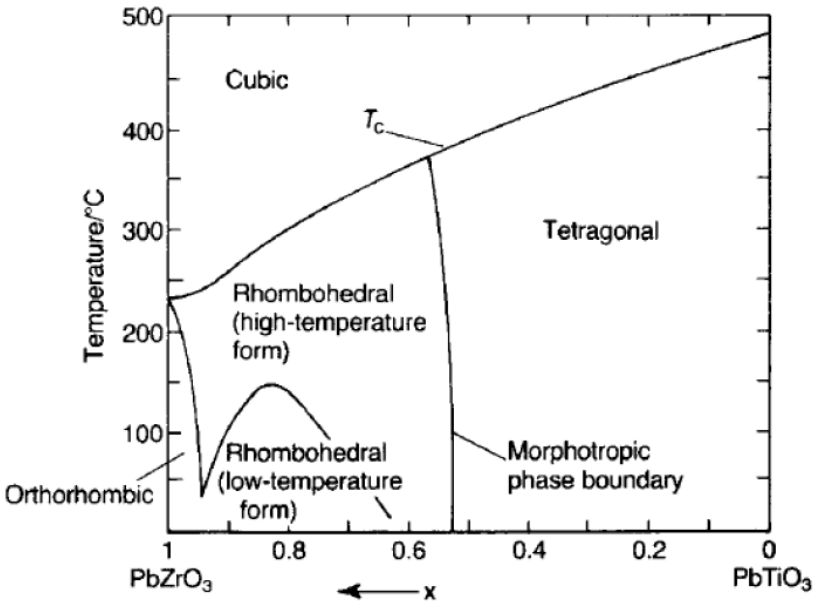

Fig. 1.6: Phase diagram of $Pb(Ti_{1-x}Zr_x)O_3$ solid solution [21]

In addition to compositional modification mentioned above, the chemical modification of PZT ceramics by doping can also greatly enhance the properties of the ceramics. The process of doping involves modifying the properties of PZT ceramics by the addition of small amount of impurities. Depending on the type of impurity added, the PZT ceramics is classified as '*Hard*' and '*Soft*' ceramics. In soft PZT ceramics, few of the A^{2+} and/or B^{4+} sites in the perovskite crystal structure (see Figure 1.3) are replaced by three valent and/or five valent cations, such as La^{3+} and Nb^{5+} (i.e. donor doping), respectively, resulting in the formation of cationic vacancies at the A and/or B sites. Due to the presence of cationic vacancies, the domain walls move easily, resulting in lower coercive field. This further makes the poling process of soft PZT much easier and more effective and also leads to better dielectric and piezoelectric properties compared to that of undoped PZT ceramics [1, 37]. On the other hand, the hard PZT ceramics are obtained by replacing few of the B^{4+} cations by lower valent cations, such as Fe^{3+} and Ni^{2+} (i.e. acceptor doping), resulting in the formation of anionic vacancies within the crystal structure of the PZT ceramic. Due to this, the domain walls get pinned to the oxygen vacancies and consequently, the hard PZT ceramics are difficult to pole and thus show lower piezoelectric properties [5, 38]. However, hard PZT ceramics are preferred in the applications that require high *Curie* temperature and mechanical quality factor. Since soft PZT ceramics are commonly applied for sensing applications, due to its superior piezoelectric properties compared to that of its counterpart, the PZT ceramics used in this research will be doped with Nb^{5+}.

1.5.2 Piezoelectric Composites

In spite of the relatively high charge constants (d_{33}) and being excellent candidates for actuator applications, the high dielectric constant of PZT ceramics (ε_r = 1800 -

2200) reduces its voltage sensitivity (g_{33}) quite drastically. Due to this, PZT ceramics are a poor choice for sensoric applications. In addition, the high density of PZT ceramics (ρ = 7.9 g/cm^3) restricts its applications in the field of aerospace engineering. Moreover, PZT is brittle in nature, which makes it difficult to process and shape into required forms. Due to these drawbacks of PZT ceramics, the development of piezoelectric composites have gained a lot of momentum since last three decades as it possess a high coupling factor, low acoustic impedance, moderate dielectric constant and better voltage sensitivity, along with superior mechanical properties and flexibility compared to that of piezoelectric ceramics. The PZT-Polymer composites is a combination of an active piezoelectric phase and a passive polymer phase, which helps in obtaining composites with tailored and unique set of dielectric, piezoelectric and mechanical properties. The presence of passive polymer phase is responsible for providing desired properties to the piezoelectric composite material, such as increasing mechanical robustness, low density and acoustical impedance. In general, a typical two phase piezoelectric composite is classified into 10 types depending on the physical connectivity of each phase [39, 40], as shown in Fig. 1.7, with the first number denoting the connectivity of active phase and the second number refers to the passive phase. This connectivity pattern between the active and passive phase has high influence on the processing and final properties of the piezoelectric composite prepared [41].

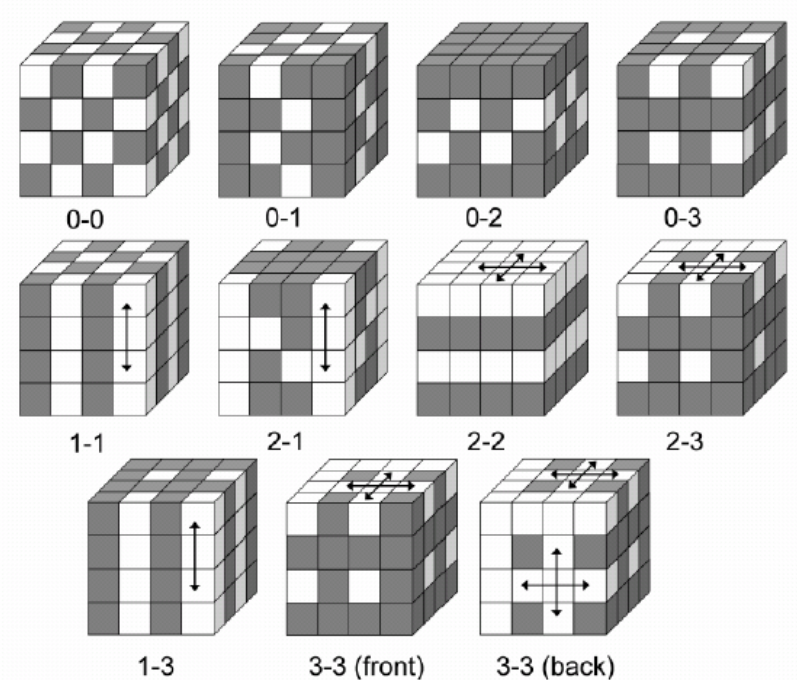

Fig. 1.7: Overview of the possible connectivity schemes between active ceramic phase (white) and passive polymer phase (grey) of two phase piezoelectric composites [40]

Among these various types of piezoelectric composites, 0-3 and 1-3 type of connectivity have received the most attention. In 1-3 composites, the ceramic phase is fully connected from

electrode to electrode, due to which this type of composites are seen as a direct replacement to bulk ceramics. Unfortunately, the superior properties of 1-3 composites come with high production costs and also suffers from performance degradation after a certain number of loading cycles [41, 42]. As an effort towards the reduction of the production cost associated with 1-3 composites, an interesting technique was developed by which piezoelectric particles/short fibers dispersed in a polymer matrix were made structured by means of dielectrophoresis process, thereby resulting in the formation of quasi 1-3 composites [30, 43]. Alternatively, 0-3 composites is the simplest of all composites and consists of randomly distributed piezoelectric ceramic particles in polymer matrix. Even though 0-3 composites exhibit lower piezoelectric properties compared to that of 1-3 composites [40], the former is relatively easy and cheap to manufacture and is thus chosen as the type of composite to be prepared as a part of this research work. A comprehensive overview regarding the various methods for making piezoelectric composites have been presented in the work of *Akdogan et al* [11]. Table 1.2 shows the dielectric and piezoelectric properties of 0-3 composites with different types of polymer phases.

Table 1.2: Overview of the dielectric and piezoelectric properties of different types of 0-3 composites

Composite	ε_r	d_{33} (pC/N)	g_{33}^* (mV.m/N)	References
0-3 PZT (70%) – Epoxy	100	45	51	[44]
0-3 PZT (60%) – Epoxy (Structured)	45	17	43	[43]
0-3 PZT (68.5%) – Carbon (1.5%) – Epoxy	120	50	47	[44]
0-3 PZT (70%) – PVDF	105	25	27	[45]
0-3 PZT (50%) – PU	48	30	71	[46]
0-3 PZT (70%) – PVDF – Fluorine Elastomer	26	10	43	[47]
0-3 $PbTiO_3$ – Rubber	45	40	100	[21]
0-3 PZT (50%) – LCT – PA (20%)	73	42	65	[48]
0-3 PZT (50%) – PA	68	28	47	[48]
0-3 PZT (40%) - LCT	30	13	49	[49]
0-3 PZT (30%) – Zn ionomer	9	5	63	[50]
0-3 PZT (30%) - EMMA	8	2	28	[50]
BNBT – P(VDF-TrFE) (70%)	21	14	75	[51]

*g33 is calculated using Eq. 1.6; PVDF - Polyvinylidene fluoride; PU – Polyurethane; LCT - Liquid Crystalline Thermoset; PA – Polyamide; EMMA - ethylene methacrylic acid copolymer; BNBT - $(Bi_{0.5}Na_{0.5})TiO_3$-$BaTiO_3$; P(VDF-TrFE) - poly[(vinylidenefluoride-co-trifluoroethylene]

1.6 Motivation and Objectives of the Thesis

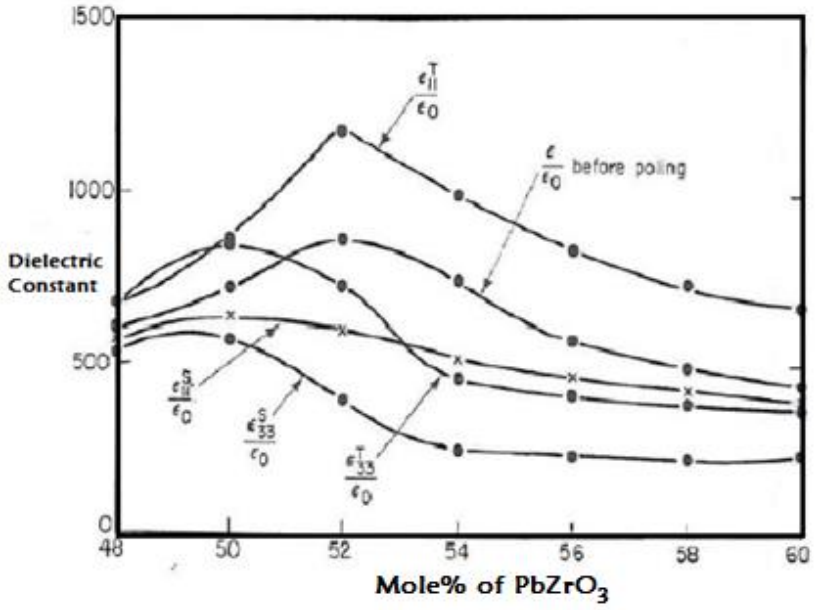

Fig. 1.8: Variation of room temperature dielectric constant (ε_r) with composition for Pb(Ti, Zr)O_3 ceramics (adapted from [1])

Most of the piezo devices are based on piezoelectric ceramics and among this, MPB composition of PZT solid solution are widely accepted for many applications. The reason behind this wide acceptance of MPB composition is the co-existence of rhombohedral and tetragonal phases, which results in an increased ease of domain orientation during poling, resulting in enhanced dielectric and piezoelectric properties. The dielectric and piezoelectric properties of MPB and close to MBP compositions of bulk ceramics have been well researched and documented by *Jaffe et al* [1]. From Fig. 1.8 and Fig. 1.9, it is noteworthy that the dielectric constant (ε_r) and piezoelectric charge constant (d_{33}) exhibits their highest values at MPB composition, while the piezoelectric voltage constant (g_{33}) maintains its high values into the rhombohedral field. The main reason which restricts the exploration of PZT phase diagram away from the neighbourhood of MPB is the poor sinterability and the poling difficulty associated with the tetragonal PZT ceramics (explained in detail in Chapter 4) and the antiferroelectric nature of the rhombohedral phase of the PZT ceramics. As far as the sensoric applications of piezoelectric ceramics are considered, the piezoelectric voltage coefficient (g_{33}) plays a major role in determining the voltage sensitivity of the ceramics. Even though the high d_{33} of MPB and close to MPB compositions of ceramics favours higher g_{33}, the very high ε_r of MPB ceramics deteriorates the final voltage sensitivity of PZT ceramics (see Eq. 1.6). Hence, in order to enhance the application of PZT ceramics as voltage sensors, it is necessary to explore the non-MPB compositions of PZT to identify a ceramic composition which would result in a

significantly higher g_{33} than that of PZT ceramics with MPB or close to MPB compositions. As a result, a systematic research is very much needed to complete the entire phase diagram of PZT (shown in Fig. 1.6) ceramics by preparing bulk ceramics of compositions $PbNb_{0.01}(Zr_xTi_{(1-x)})O_3$, for x varying from 0 to 0.80.

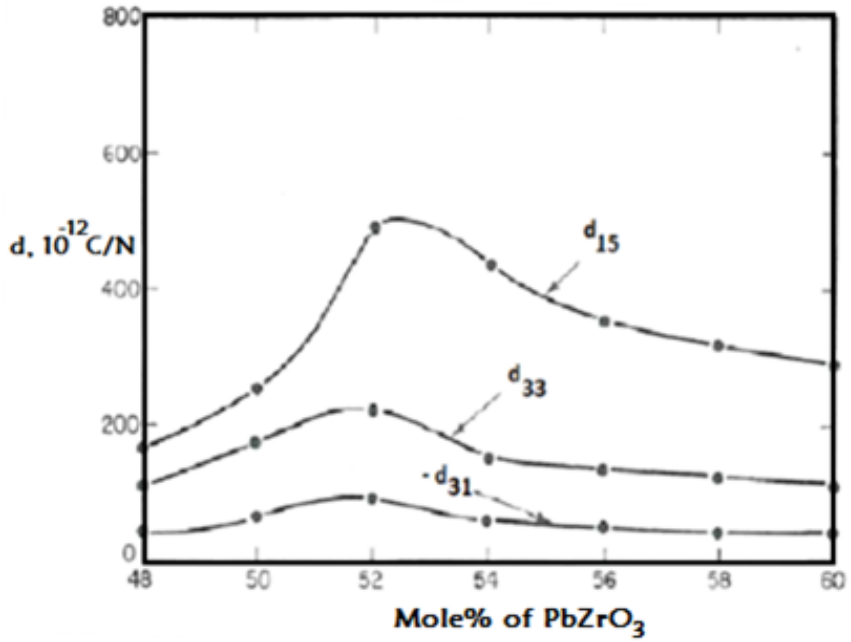

Fig. 1.9: Variation of room temperature piezoelectric charge coefficient (d_{33}) with composition for $Pb(Ti, Zr)O_3$ ceramics (adapted from [1])

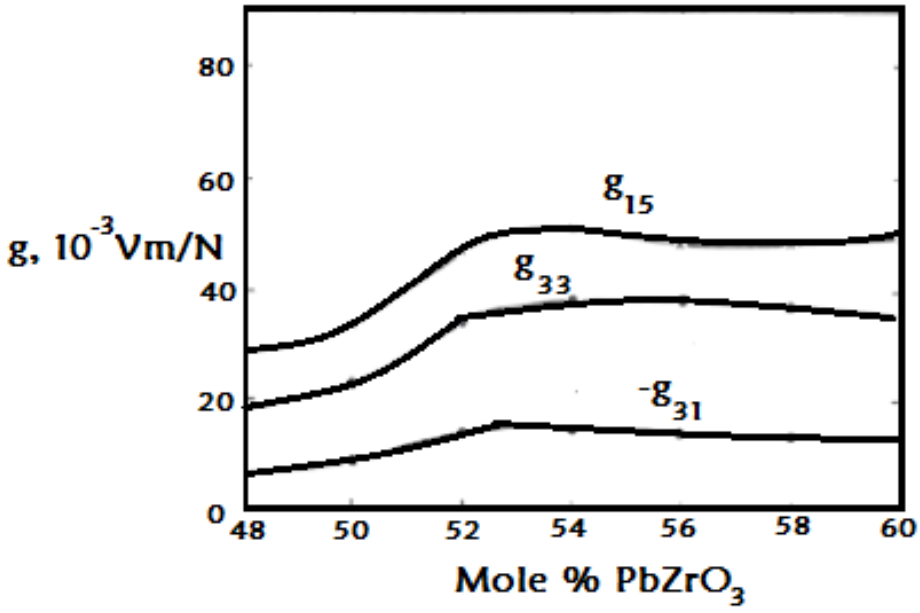

Fig. 1.10: Variation of room temperature piezoelectric voltage coefficient (g_{33}) properties with composition for $Pb(Ti, Zr)O_3$ ceramics (adapted from [1])

Unlike bulk ceramics, in which the ceramic grains are in contact with each other in all direction, in 0-3 piezoelectric-polymer composites, the high ε_r PZT ceramic filler particles having a particle size of 2-4 μm range are surrounded by a low ε_r polymer phase, with no connectivity between the filler particles. Due to this, the piezoelectric composites will exhibit entirely different poling and polarization mechanisms. Consequently, it is not necessary that the MPB or close to MPB compositions of ceramic filler particles will result in higher dielectric and piezoelectric properties. In addition, the presence of polymer phase results in a better poling process of tetragonal compositions of PZT ceramic filler particles compared to that of its bulk ceramic counterparts. Even though the lack of connectivity will result in lower d_{33}, the significantly lower effective ε_r results in an enhanced g_{33} in composites, which enable these composites to be used for various potential applications such as pressure sensors and strain-energy harvesting. As a result, efforts will be made in this research work in exploring the effect of non-MPB PZT compositions as fillers in 0-3 composites.

Based on the above prospects expected from the 0-3 piezoelectric composites, the following objectives have been formulated which would be investigated during the course of this research work:

- Investigate the possibilities of using non-MPB PZT compositions as the filler materials in 0-3 PZT-Polymer composites in order to maximize the voltage sensitivity (g_{33}) of the piezoelectric composites

- study the effect of dielectric constant of ceramic filler on the dielectric and piezoelectric properties of the PZT-Polymer composites prepared

- Inspect the effect of depolarization factor due to the ceramic on piezoelectric charge constant (d_{33}) of 0-3 PZT-Polymer composites

- Propose certain material selection criteria for preparing 0-3 piezoelectric composites with good sensorial properties.

2. Experimental

2.1 Introduction

As far as the preparation of 0-3 composite materials are considered, there are several factors, which will have an influence on its final properties such as the dielectric and piezoelectric properties of the constituent materials, poling conditions, filler volume fraction, filler grain size, density, porosity and poling conditions. Thus it is necessary to follow the above factors while preparing the composites in order to have a better repeatability.

In this chapter, the procedure for the preparation of $PbNb_{0.01}[Zr_xTi_{(1-x)}]O_3$ ceramic powder, sintered ceramic disks and 0-3 composites are discussed in detail initially. Secondly, various characterization techniques adopted to study the microstructure and dielectric properties of PZT ceramics are given in following sections. Finally, the 0-3 composites prepared were analyzed with respect to their microstructure, P-E hysteresis, dielectric and piezoelectric properties and electric fatigue response.

2.2 Processing of Ceramic Powder and Ceramic Disks

2.2.1 Ceramic Powder

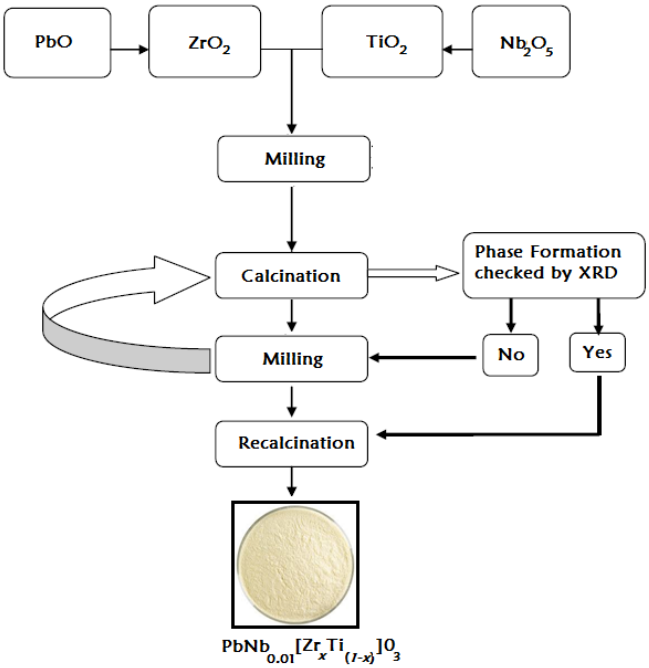

Fig. 2.1: Flow chart for the preparation of $PbNb_{0.01}[Zr_xTi_{(1-x)}]O_3$ by solid state reaction process

Among the various techniques available [52, 53], the most conventional and economical mixed oxide process (also known as solid state reaction process) was used to synthesize the $PbNb_{0.01}[Zr_xTi_{(0.99-x)}]O_3$ ceramic powder and Table 2.1 shows the list of ceramic compositions prepared. Henceforth, the compositional codes mentioned in Table 2.1 will be used in the subsequent sections.

Table 2.1: $PbNb_{0.01}[Zr_xTi_{(1-x)}]O_3$ compositions prepared and the corresponding compositional codes

Zr mole% (x)	Powder Composition	Composition Code
0	$PbNb_{0.01}Ti_{0.99}O_3$	PT
10	$PbNb_{0.01}(Ti_{0.89}Zr_{0.10})O_3$	PZT – 10
20	$PbNb_{0.01}(Ti_{0.79}Zr_{0.20})O_3$	PZT – 20
30	$PbNb_{0.01}(Ti_{0.69}Zr_{0.30})O_3$	PZT – 30
35	$PbNb_{0.01}(Ti_{0.64}Zr_{0.35})O_3$	PZT – 35
40	$PbNb_{0.01}(Ti_{0.59}Zr_{0.40})O_3$	PZT – 40
45	$PbNb_{0.01}(Ti_{0.54}Zr_{0.45})O_3$	PZT – 45
50	$PbNb_{0.01}(Ti_{0.49}Zr_{0.50})O_3$	PZT – 50
52	$PbNb_{0.01}(Ti_{0.47}Zr_{0.52})O_3$	PZT – 52 (MPB)
54	$PbNb_{0.01}(Ti_{0.45}Zr_{0.54})O_3$	PZT – 54
60	$PbNb_{0.01}(Ti_{0.39}Zr_{0.60})O_3$	PZT – 60
70	$PbNb_{0.01}(Ti_{0.29}Zr_{0.70})O_3$	PZT - 70
80	$PbNb_{0.01}(Ti_{0.19}Zr_{0.80})O_3$	PZT - 80

The lead oxide (PbO), zirconia (ZrO_2), titania (TiO_2) and niobium pentoxide (Nb_2O_5) from Sigma Aldrich, with 99.9% purity, were used as the raw materials. The raw materials were weighed according to the stoichiometric proportions based on the desired ceramic

composition. In order to attain homogeneity, the raw materials were thoroughly milled with 5-mm zirconium balls for 7 hrs in distilled water. The mixture was then dried using hot air oven in order to evaporate the distilled water. The dried powder was then calcined in a furnace using a closed alumina crucible at 750°C for 2 hrs at a heating rate of 2°C/min in order to initiate the formation of perovskite phase. The calcined powders were crosschecked for phase formation by X-ray diffraction technique. Once the phase formation was observed the powder was milled again as mentioned above for 3 hrs and was dried in a hot air oven for overnight at 120°C. The dried powder was calcined again at 1150°C for 2 hrs at a heating rate of 2°C/min. The flow chart depicting the formation of ceramic powder by solid state reaction is shown in Fig. 2.1. The crystal structure and phase formation of the ceramic powders were determined using X-ray diffraction technique, which will be explained in the Section 2.4.

2.2.2 Ceramic Disks

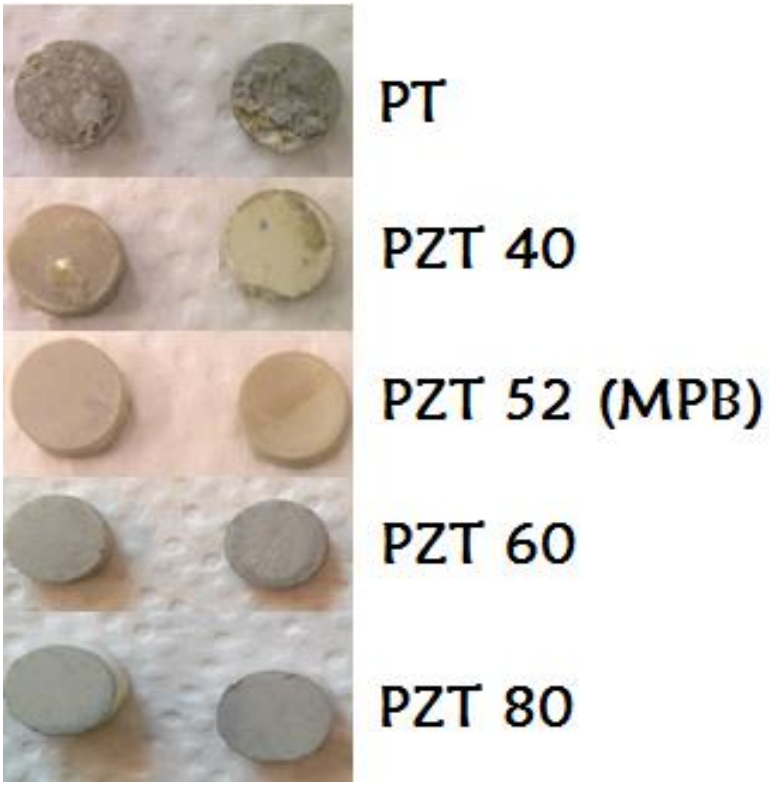

Fig. 2.2: Photographs of sintered $PbNb_{0.01}[Zr_xTi_{(1-x)}]O_3$ ceramics with x = 0, 0.40, 0.52, 0.60 and 0.80

In order to investigate the dielectric and piezoelectric properties of ceramics, four to five sintered ceramic disks were prepared by pellet-pressing. Prior to the pressing of ceramic disk, Polyvinyl alcohol (PVA) was used as a binder in order to reduce the brittleness of the disks. The fine and homogeneous ceramic powder was pressed into cylindrical disks of 6.5 mm diameter and 1.5-2.5 mm thickness under an uniaxial pressure of $5x10^5$ N/m2 using a hydraulic

press. The pressed ceramic disks were sintered for 2 hrs at 1250°C on a bed of commerically avaiable PZT powder using a high temperature furnace. From Fig. 2.2, it can be seen that the ceramic disks with high Ti content (resulting in high tetragonality) such as PT and PZT 40 displayed poor sinterability, which made the poling process impossible. The reason behind this poor sinterability will be discussed in detail in Chapter 4.

2.3 Epoxy Thermoset Polymer

The two component epoxy system used for the preparation of 0-3 composites is a two component – *Epotek 302-3M Epoxy (diglycidyl ether of bisphenol-A) resin* and *poly(oxypropyl)-diamine multifunctional aliphatic amine curing agent.* The chemical structure of the resin and curing agent is as shown in Fig. 2.3. The dielectric constant of the cured Epoxy matrix is estimated to be 4.2 and the polymer possesses excellent dimensional stability upto a temperature of 100°C. As a result, the poling temperature of the 0-3 composite prepared using epoxy polymer has been set as 80°C.

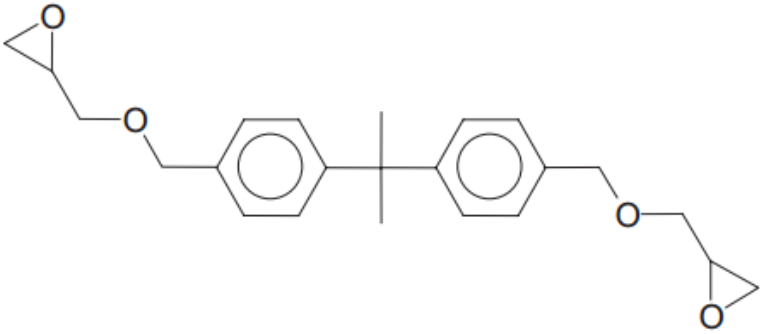

(a)

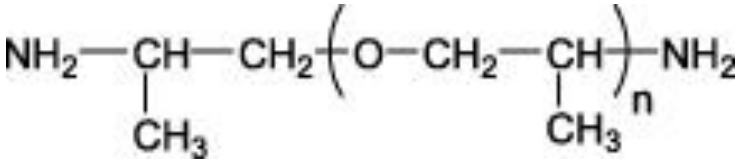

(b)

Fig. 2.3: Chemical structure of (a) diglycidyl ether of bisphenol-A resin [54] and (b) Poly(oxypropylene) diamine curing agent [55]

2.4 Processing of 0-3 PZT–Epoxy Composites

The 0-3 composites were prepared by tape-casting method by following the steps as shown in the Fig. 2.3. The ceramic filler particles were initially dispersed in the resin component of the epoxy and mixed at 3000 rpm for 5 min using a planetary mixer (SpeedMixer DAC 150.1 FVZ). The slurry thus obtained was degassed for 5 min. Subsequently, the curing agent was

added to the mix of resin and ceramic particles and was mixed at 2000 rpm for 5 min. Finally the composite slurry was degassed for 5 min in order to remove air bubbles. Subsequently, the composite slurry was deposited on a thin aluminium foil and tape-casted using a movable header at a speed of 2 m/s, resulting in the formation of around 200 micron thin sheets of 0-3 PZT Epoxy composites, as shown in Fig.2.4. For each variation of $PbNb_{0.01}[Zr_xTi_{(1-x)}]O_3$ ceramic powders synthesized, 20 and 40 vol% of ceramic filler-epoxy composites were prepared. The composites thus formed were cured at room temperature for 24 hrs. After curing, the composites samples were cut into thin circular disks of 12 mm diameter using a circular punch.

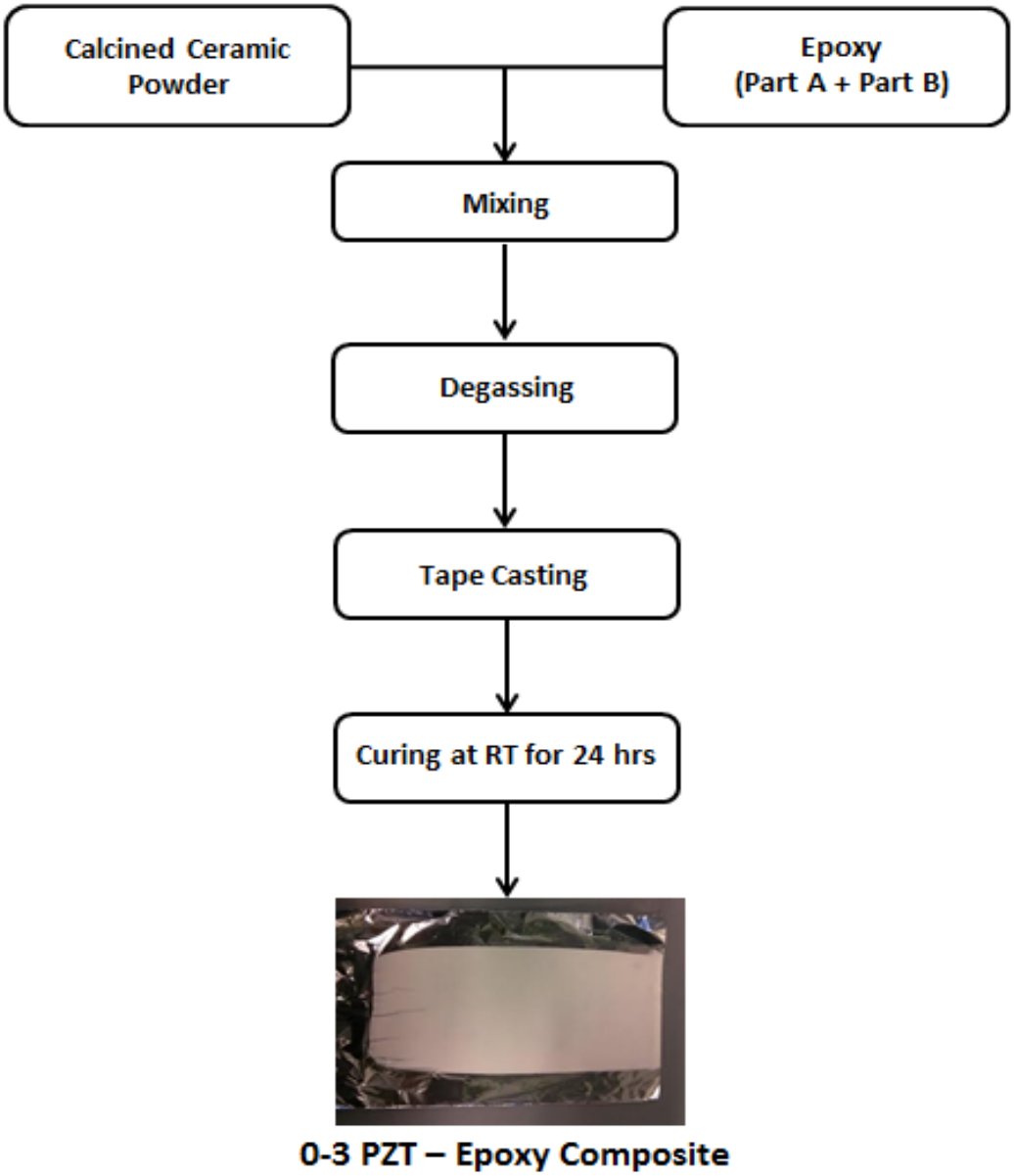

Fig. 2.4: Flow chart for 0-3 PZT – Epoxy Composite processing

2.5 Phase Analysis and Microstructure Characterization

2.5.1 X-ray Diffraction (XRD)

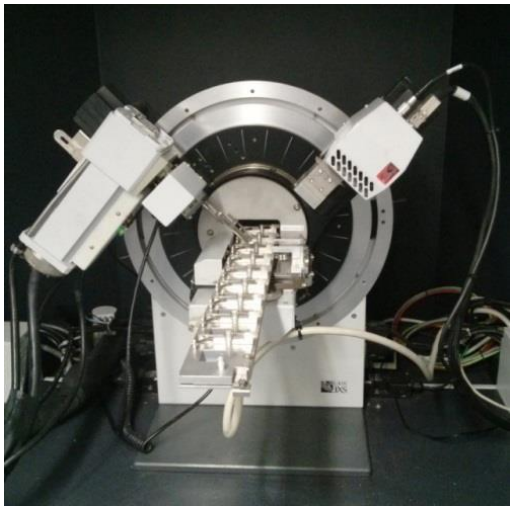

Fig. 2.5: Bruker D8 ADVANCE X-ray Diffractometer

The phase purity and lattice parameters of the calcined $PbNb_{0.01}[Zr_xTi_{(1-x)}]O_3$ ceramic powders were examined using X-Ray diffraction. The fine powdered ceramic samples were analysed using Bruker D8 ADVANCE X-ray Diffractometer, shown in Fig.2.5, using Co-Kα radiation of wavelength 1.79 Å. The XRD experiment was carried out at room temperature for a two theta (2θ) from of 5° to 70°, using a step size of 0.02° and a scan step of 1 s. The XRD data obtained were further analysed using PANalytical X'Pert HighScore Plus, Version 2.0, to determine the lattice parameters of each compositions of $PbNb_{0.01}[Zr_xTi_{(1-x)}]O_3$ ceramic powder.

2.5.2 Particle Size Analysis

Fig. 2.6: Beckman Coulter LS 230 particle analyser

The laser diffraction technique was used to determine the particle size distribution of the calcined ceramic powder using Beckman Coulter LS 230 particle analyser (shown in Fig. 2.6) at a laser wavelength of 750 nm at Kramers laboratory of DelftChemTech. Prior to the analysis, the calcined powder was mixed with distilled water and sodium pyrophosphate (dispersion medium). The resulting solution was then ultrasonicated for 5 min in order to free the powder from agglomerates.

2.5.3 Scanning Electron Microscopic (SEM) Analysis

Fig. 2.7: Scanning Electron Microscopy (SEM) JEOL JSM 840A

The microstructural analysis of the ceramic powders and the cross sections of ceramic disks and composites were carried out using a scanning electron microscope (JEOL – JSM 840A), shown in Fig. 2.7. The specimens were gold coated prior to being analysed using SEM in order to facilitate imaging, as the specimens are non-conducting.

2.6 Poling of 0-3 PZT–Epoxy Composites

The room temperature cured circular disk-shaped 0-3 PZT-epoxy composite specimens were post-cured at 120°C in order to remove moisture. The gold electrodes of 9 mm were deposited on the Aluminium-free side of post-cured composite specimens using Balzers Union Sputtering System SCD 040. The electroded composite samples were poled at 15 kV/mm at 80°C in silicon oil bath for 1 hr. The samples were then cooled down to 30°C in the presence of

poling field and was allowed to age for 24 hrs before measuring the dielectric and piezoelectric properties. Fig. 2.8 shows the set-up used for the poling process.

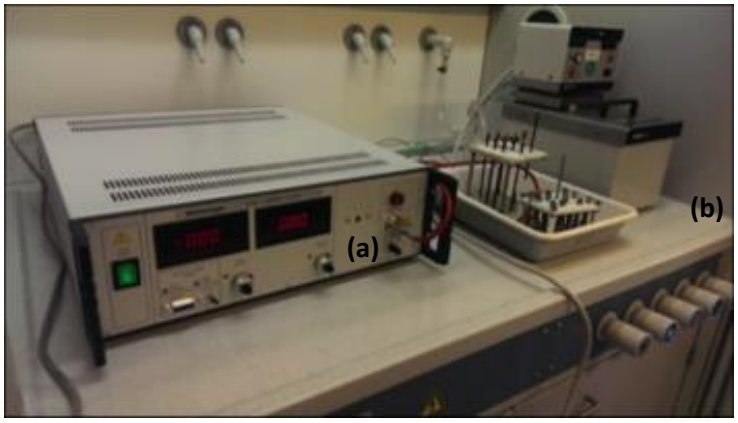

Fig. 2.8: Set-up for poling process: (a) High voltage amplifier and (b) Silicon oil bath

2.7 P-E Hysteresis and Polarization Fatigue Measurement

Fig. 2.9: Piezoelectric hysteresis and polarization fatigue measurement set-up

The P-E hysteresis loop measurements were carried out to determine the remnant polarization (P_r), spontaneous polarization (P_s) and coercive field (E_c) of the 0-3 composites prepared. The experiments were carried out at room temperature at an applied field range from 1 to 600 kV/cm, using a standardized ferroelectric measurement test system of Radiant Technology (Version 5.0.3), at Max Planck Institute for Polymer Research at Mainz, Germany. The room temperature polarization fatigue measurements were carried out using Radiant Technology (Version 4.0.5), as shown in Fig. 2.9, at the Physical Lab of Aerospace and Structures Department at Delft.

2.8 Measurement of Dielectric and Piezoelectric Properties

Fig. 2.10: Berlincourt d_{33} meter (a) and LCR meter (b)

The dielectric constant of the ceramic disks and composites were measured using the parallel plate capacitor method using an Agilent 4263B LCR meter at 1 V and 1 kHz. The piezoelectric charge constant (d_{33}) of the composites were performed using a Berlincourt type d_{33} meter and the measurements were carried out at a standard static force of 10 N and frequency of 110 Hz. Fig. 2.10 shows the equipment used to measure the dielectric and piezoelectric properties.

3. Modelling of Dielectric and Piezoelectric Properties

3.1 Introduction

Piezoelectric ceramic-polymer composites are being increasingly used for sensor and actuator applications [11, 56]. The piezoelectric composites consists of high dielectric constant ceramic particles embedded (randomly or structured) in a low dielectric polymer matrix, exhibiting good mechanically flexibility, easy formability, low density and low dielectric losses [42, 57]. The major factors which determine the final properties – dielectric and piezoelectric coefficients – of these composites are as follows [58]:

I. Properties of the constituent phases *i.e. ceramic and polymer phase*
II. Volume fraction and connectivity of the constituent phases

Apart from above mentioned dominant factors, the interfacial interaction between the ceramic particles and polymer matrix, percolation and porosity also have an influence of the final dielectric and piezoelectric properties of the composites. [57, 59]. Considering 0-3 composites, the geometry of the inclusions also affects the final properties of the composite [60]. Thus, many theoretical models were developed in order to predict the dependence of dielectric and piezoelectric coefficients of the composites as a function of volume fraction of filler particles, dielectric constant of constituent phases and interaction between the constituent phases.

In this chapter, a review on most widely used analytical models for predicting the dielectric and piezoelectric coefficients of 0-3 composites are presented. The five different analytical models selected – *Mixture Rule Models [61] , Furukawa Model [62] , Maxwell Wagner Model [63, 64] , Jayasundere Model [65] and Yamada Model [47]* – were based on the works on dielectrics models for ceramic-polymer composites by *Araújo et al* [57]. The models discussed in this chapter were also used to compare and validate the experimental results, which will be explained later in Chapter 4.

3.2 Mixture Rule Models

Among the various reported mixture rule models, exponential mixture and logarithmic mixture are the most widely studied rules and thus will be further investigated in the following sections. The mixture rules are derived based on the assumption that the filler particles are uniformly distributed in a continuous matrix and no interactions between these constituents are taken into account [57, 61].

3.2.1 Exponential Mixture Rule

Using above mentioned assumptions, the dielectric constant of composite containing dielectric fillers embedded in a polymer matrix can be expressed as:

$$(\varepsilon_c)^k = V_f(\varepsilon_f)^k + (1-V_f)(\varepsilon_m)^k \quad (3.1)$$

where ε_c, ε_f and ε_m are the dielectric constants of the composite, pure ceramic filler and polymer matrix respectively, *k* is an empirical parameter that depends on shape and orientation of the filler particles and V_f is the volume fraction of the filler medium. In general, the value of *k* corresponds to -1 (series model) or 1 (parallel model), with the former being derived by considering the total capacitance (which is later on used to derive dielectric constant) of the composite as the sum of two capacitances in series connection whereas *k*=1 corresponds to parallel connection. In addition, a mixture model for randomly dispersed ceramic filler particles was also derived for which the value of *k* corresponds to 1/3 and is termed as random model. Apart from above mentioned three exponential mixture models with constant *k* value, a modified empirical equation was proposed by Wakino for *k* (shown in Eq. 1.9) with an assumption based on non-aspect and random dispersion of filler particles in polymer matrix.

$$k = V_f - 0.35 \quad (3.2)$$

The value of k for series and parallel model are two extreme cases (known as Wiener boundary values) and thus is expected to have poor accuracy when compared with that of experimental values. But in case of random model, the value of *k* = 1/3 is closer to the physical condition and thus provides a better accuracy than that of series and parallel models. The limitation of exponential mixture rule is that these set of mixture rules are compatible only with higher volume percentage of filler materials [61].

3.2.2 Logarithmic Mixture Rule

Another important mixing rule is Lichtenecker's logarithmic mixing rule and is considered as the inverse of the exponential rules. The logarithmic rule follows the same assumptions as that of exponential mixture rules but the value of *k* is determined from the

experimental data. Hence the Lichtenecker's rule is regarded as semi-empirical in nature and is given by the following equation [66, 67]:

$$\log \varepsilon_c = V_f \log \varepsilon_f + (1 - V_f) \log \varepsilon_m \qquad (3.3)$$

The main drawback of Lichtenecker's rule is that it has been derived on the basis of fitting to the empirical data and lacks a physical model. In addition, the mixing rule can be applied only if ε_f differs slight from ε_m. In spite of these drawbacks, the logarithmic mixture rule has proven to be a useful formulation for the determination of the effectivity dielectric constant of composites [64, 68].

3.3 Furukawa Model

Furukawa studied a two phase system composed of spherical inclusion (i.e. ceramic filler) embedded in a polymer matrix, which in turn is covered with a homogeneous medium whose properties approximate the average composite properties, as shown in Fig. 3.3. Using above mentioned conditions, Furukawa formulated following equations for the dielectric and piezoelectric coefficients of 0-3 composites [69]:

$$\varepsilon_c = \frac{(1 + 2V_f)}{(1 - V_f)} \varepsilon_m \qquad (3.4)$$

$$(d_{33,c}) = \frac{15V_f}{(2 + 3V_f)(1 - V_f)} \frac{\varepsilon_m}{\varepsilon_f} (d_{33,f}) \qquad (3.5)$$

$$(g_{33,c}) = \frac{15V_f}{(1 + 2V_f)(2 + 3V_f)} (g_{33,f}) \qquad (3.6)$$

where V_f is the volume fraction of ceramic filler, d_{33} and g_{33} are the piezoelectric charge constant and voltage constants respectively and ε is the dielectric constant with the subscripts *f* and *m* corresponding to that of ceramic and polymer phase respectively ($\varepsilon_f >> \varepsilon_m$). The main drawback of Furukawa model is that no interactions between the constituent phases are taken into consideration while formulating the equations since the model assumes that the composite is electrically homogeneous. But this may not be true in case of a two-phase composite system due to the space charge effects (i.e. Maxwell-Wagner effect)[70].

3.4 Maxwell–Wagner Model

Maxwell proposed a simple model for determining the effective dielectric constant of randomly distributed non-interacting particles in a polymer matrix, given by Eq. 1.14. The model assumes that the particles are well dispersed in the polymer matrix and the potential around each filler particle do not have any influence on surrounding particles as most of them are not touching each other. This assumption of Maxwell-Wagner model restricts its application to composites with low filler concentration. Another limitation of this model is that it is generally valid when the properties of the two phases in the composite are similar [71]. In spite of its drawbacks, Maxwell-Wagner model has been widely used for the calculation of the dielectric constant of filler-polymer composites [72].

$$\varepsilon_c = \varepsilon_m \frac{2\varepsilon_m + \varepsilon_f + 2V_f(\varepsilon_f - \varepsilon_m)}{2\varepsilon_m + \varepsilon_f - V_f(\varepsilon_f - \varepsilon_m)} \tag{3.7}$$

3.5 Jayasundere Model

Jayasundere and Smith developed an analytical expression for effective dielectric constant (ε_c) and piezoelectric charge coefficient ($d_{33,c}$) (given by Eq. 1.15 and 1.16) for a 0-3 composite by considering a model which consists of piezoelectric particles randomly distributed in a dielectric medium and subjected to the condition $\varepsilon_f >> \varepsilon_m$, where ε_f and ε_m are the dielectric constants of the filler and the surrounding dielectric medium respectively. Unlike previously mentioned models, Jayasundere model takes into consideration of the electric field interactions between the filler particles, which are assumed to be spherical in shape [73].

$$\varepsilon_c = \frac{V_m\varepsilon_m + V_f\varepsilon_f\left(\frac{3\varepsilon_m}{\varepsilon_f + 2\varepsilon_m}\right)\left(1 + \frac{3V_f(\varepsilon_f - \varepsilon_m)}{\varepsilon_f + 2\varepsilon_m}\right)}{V_m + V_f\left(\frac{3\varepsilon_m}{\varepsilon_f + 2\varepsilon_m}\right)\left(1 + \frac{3V_f(\varepsilon_f - \varepsilon_m)}{\varepsilon_f + 2\varepsilon_m}\right)} \tag{3.8}$$

$$(d_{33,c}) \approx (d_{33,f})\frac{\varepsilon_c}{\varepsilon_f}\left(1 + \frac{3V_f\varepsilon_f}{2\varepsilon_m + \varepsilon_f}\right) \tag{3.9}$$

The Jayasundere model is not applicable for 0-3 composite with high volume fractions of ceramic fillers (V_c > 0.70) because of the presence of some 1-3 connectivity associated with the ceramic phase [73].

3.6 Yamada Model

Yamada studied the binary system consisting of PZT powder embedded in a PVDF polymer matrix and proposed a model to explain the behaviour of the properties of the composite using the properties of its constituent materials. The model consists of ellipsoidal particles dispersed in a continuous polymer medium, as shown in Fig. 3.6, and the permittivity (ε_c) and piezoelectric charge coefficient ($d_{33,c}$) of the composite was given as follows [47, 58]:

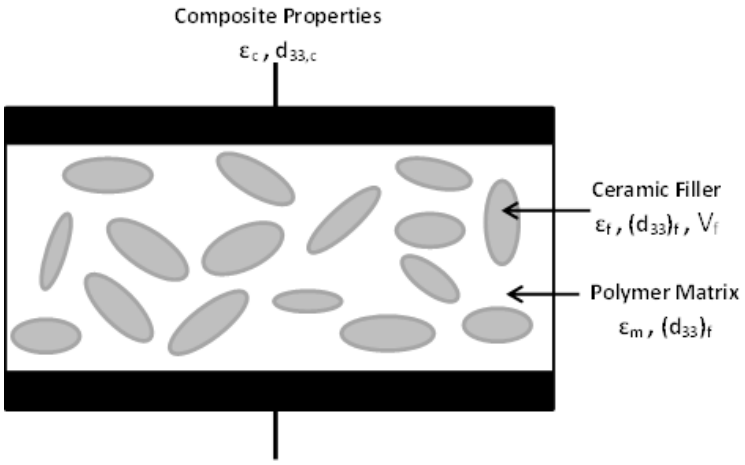

Fig. 3.1: Binary system consisting of piezoelectric ellipsoidal particles dispersed in a continuous medium (adapted from [58]).

$$\varepsilon_c = \varepsilon_m \left(1 + \frac{n V_f (\varepsilon_f - \varepsilon_m)}{n\varepsilon_m + (\varepsilon_f - \varepsilon_m)(1 - V_f)} \right) \tag{3.10}$$

$$(d_{33,c}) = \frac{V_f \varphi n \varepsilon_c (d_{33,f})}{n\varepsilon_c + \varepsilon_f - \varepsilon_c} \tag{3.11}$$

where *n* is the shape factor (depends on the geometry of the filler particles and its orientation with respect to the surface of the composite), φ is the ceramic poling ratio, V_f is the volume fraction of the filler particles and ε is the dielectric constant with the subscripts *c, f* and *m* corresponding to the properties of composite, ceramic filler and polymer matrix.

A prediction of dielectric constant for 0-3 PZT-Epoxy composite for varying PZT volume fractions is shown in Fig 3.2. The dielectric constant of the polymer matrix was measured as ε_m=4.2 and the dielectric constant of the PZT ceramic filler particles were ε_f = 1085 (MPB composition was taken as an example). Among these analytical models, the Series and Parallel models act as the lower and upper boundary for the values of dielectric constant of composites between 0-3 and 1-3 composites respectively and all the predicted as well as the experimentally determined values of dielectric constant of composites reported till date lies within these two boundaries. All the models studied in this chapter have several parameters in

common such as dielectric constant of the ceramic and polymer phase, d_{33} of ceramic fillers and volume fraction of the ceramic fillers. Apart from these, Yamada Model takes into consideration of the shape factor of the filler particles and poling ratio of the composites while predicting the dielectric and piezoelectric properties of the composites. Another important model to be considered is the Maxwell-Wagner model. This model is derived by taking into consideration of the depolarization effect caused due to the presence of two dielectric mediums (ceramic and polymer) in a system. Hence, Yamada and Maxwell-Wagner are among the most widely used analytical models, to predict the dielectric and piezoelectric properties of composites. However, the actual dielectric and piezoelectric properties of the 0-3 composite depend on many other parameters, including the degree of interaction between the filler and the matrix, homogeneity of the ceramic particle dispersion in the matrix and the precise connectivity of the filler particles at high volume fractions.

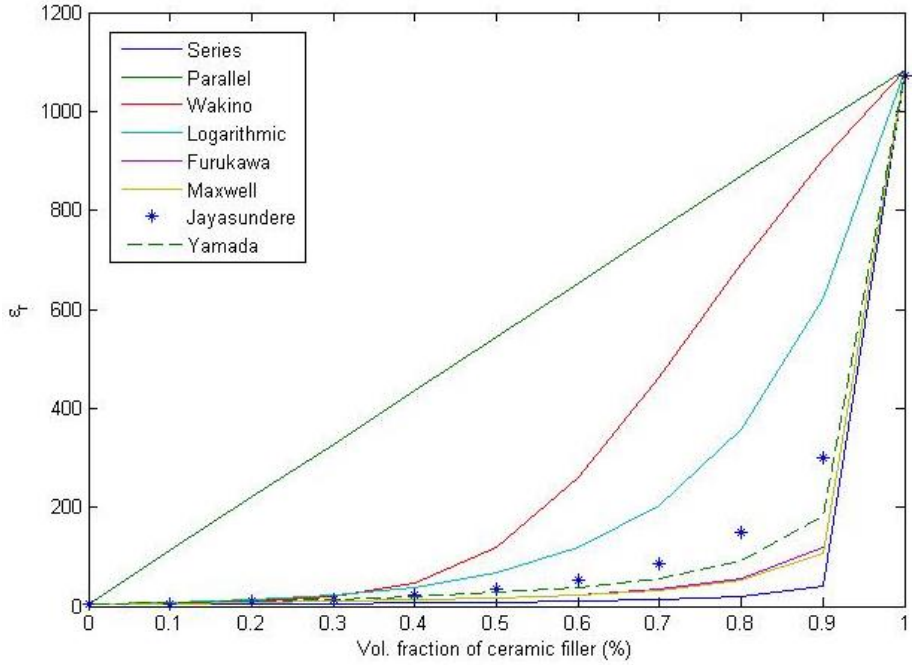

Fig. 3.2: Analytical model predictions for dielectric constant of composite as a function of vol. fraction of ceramic filler

4. Results and Discussions

This section discusses the experimental data, its interpretation and comparison with the analytical models. The results of the microstructural analysis are presented from Section 4.1, followed by the P-E Hysteresis measurement in Section 4.2. Finally the outcome of the experimental measurement of dielectric and piezoelectric properties of ceramics and composites are presented and compared with that of the analytical models in Section 4.3.

4.1 Phase Analysis and Microstructure Characterization

4.1.1 X-ray Diffraction (XRD)

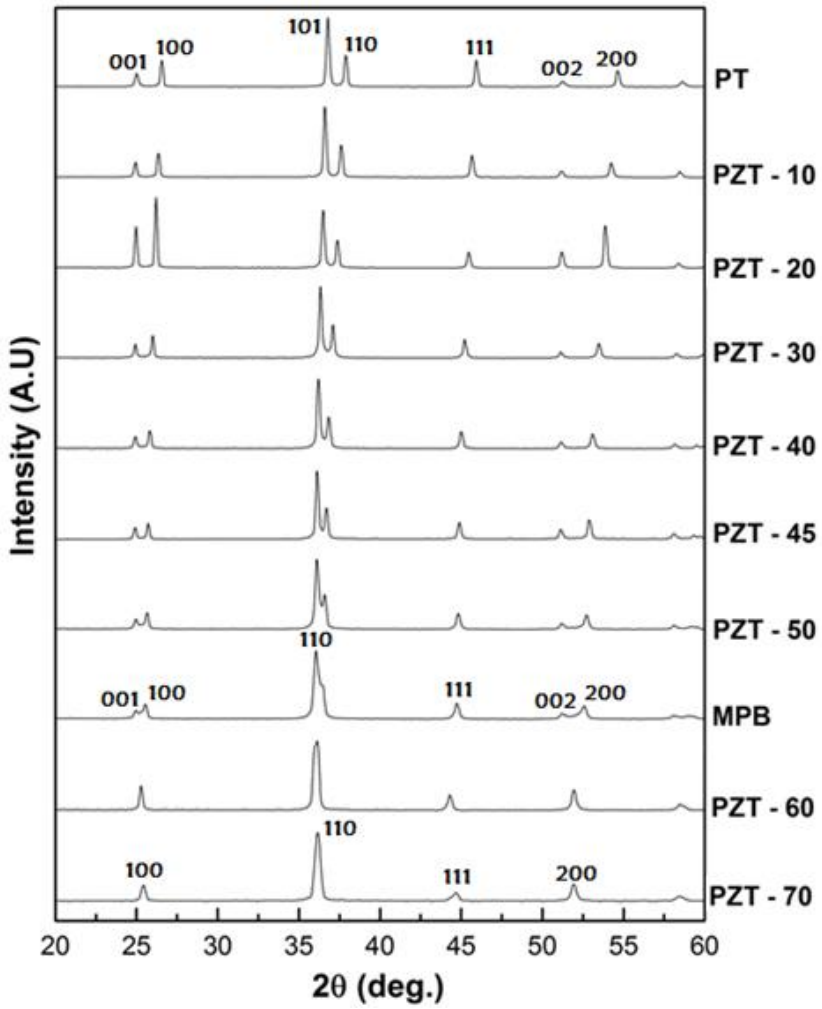

Fig. 4.1: X-ray diffraction pattern of calcined $PbNb_{0.01}[Zr_xTi_{(1-x)}]O_3$ ceramic powder

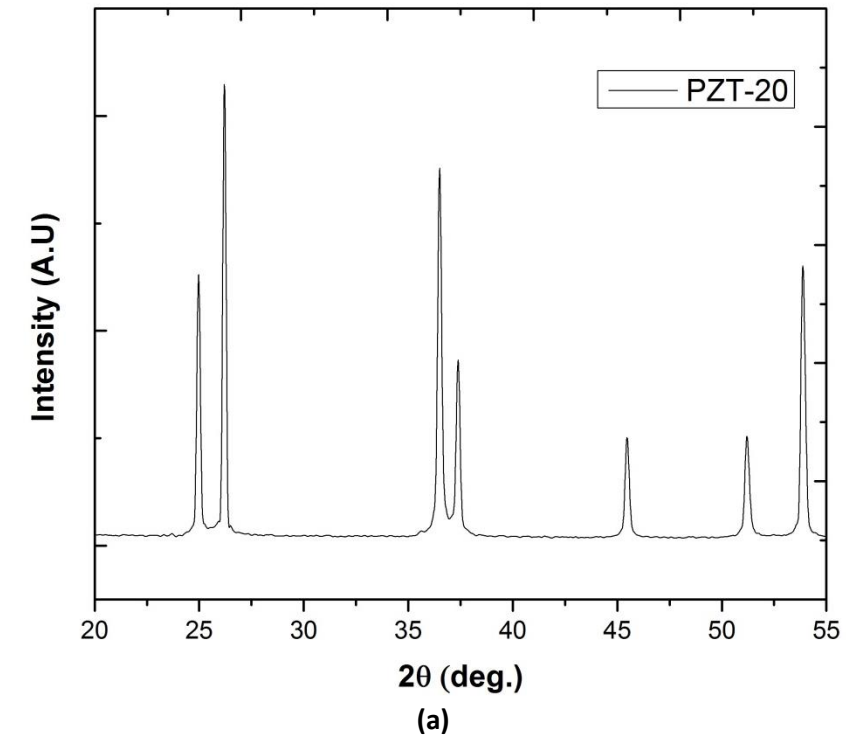

(a)

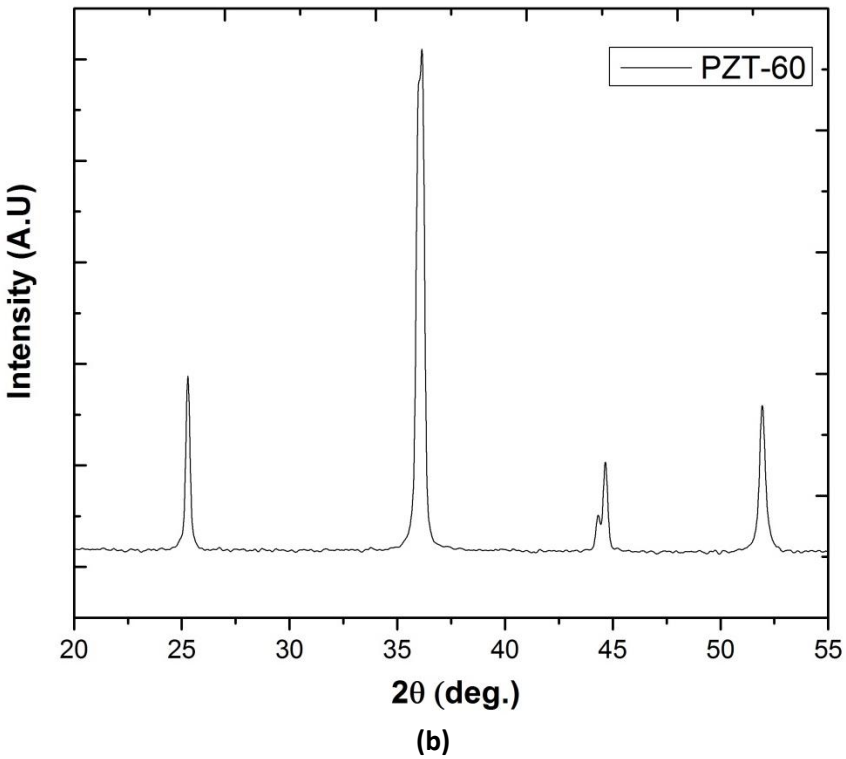

(b)

Fig. 4.2: X-Ray Diffraction of calcined ceramic powder exhibiting single phase formation: (a) PZT-20 and (b) PZT-60

The room temperature X-ray diffraction patterns of Nb-doped $PbNb_{0.01}[Zr_xTi_{(1-x)}]O_3$ as a function of Zr composition are shown in Fig. 4.1. The sharp and well defined single phase diffraction peaks confirms the formation of perovskite structure in all PZT ceramic powder compositions. The phases were identified by the analysis of the XRD patterns within the two theta (2θ) range from 20° to 60°. Within this range, (100), (110), (111) and (200) crystallographic planes experienced a shift in their 2θ position with varying Zr/Ti ratio. This systematic shift in the position of 2θ with respect to Zr composiion ratio indicates the transformation from rhombohedral (PZT-80) to tetragonal phase. The splitting of (002) reflection into (002) and (200) reflections at PZT-52 (MPB i.e. x=0.52) indicates the presence of morphotropic phase boundary (MPB) region, at which the co-existence of the tetragonal and rhombohedral phases are observed. The reason behind this splitting of reflections at MPB region can be attributed to the compositional fluctuations, leading to the coexistence of the rhombohedral and tetragonal phases [74-76]. It can also be seen that when Zr/Ti < 52/48, the diffractograms exhibit distinct split peaks at (101) and (110), which denotes the tetragonal phase composition of the ceramic powder. In addition, with the increase in the tetragonal phase, the (111) peak becomes more distinct. Thus, from the diffraction pattern it can be seen that all the compositions were of pure perovskite structure and observed the rhombohedral to tetragonal phase transformation of PZT ceramic powder as the Zr composition decreases. Fig 4.2 shows the full sized diffraction pattern of PZT-20 and PZT-60 compositions in order to highlight phase purity and single phase formation.

4.1.2 Lattice Parameter

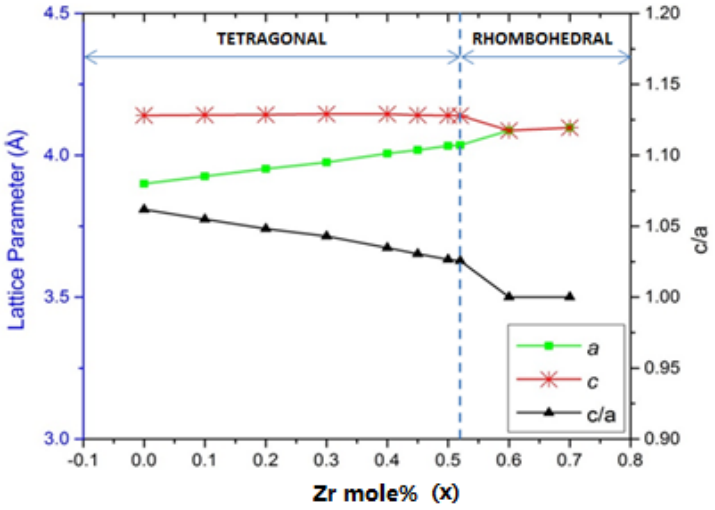

Fig. 4.3: Lattice parameters and *c/a* ratio of calcined $PbNb_{0.01}[Zr_xTi_{(1-x)}]O_3$ ceramic powder

Fig. 4.3 shows the variation of lattice constants `*a*' and `*c*' and *c/a* ratio as a function of the Zr mole%. The *c/*a ratio for MPB composition of PZT was found to be 1.025 whereas that of $PbTiO_3$ was 1.062. Even though the lattice constant 'c' remains almost constant, an increase in lattice constant '*a*' is observed, thereby leading to a reduction in *c/a* ratio with increase in Zr

content. This reduction in c/a ratio indicates that the tetragonality of PZT ceramics decreases with increase in Zr content and these values of the lattice parameters were found to be close to ones which were reported previously [77].

4.1.3 Particle Size Analysis

The particle size distribution of the calcined $PbNb_{0.01}[Zr_xTi_{(1-x)}]O_3$ ceramic powders, for *x* = 0 to 0.8, were measured using laser diffractometry. Since the particle size of the ceramic filler have an influence on the dielectric and piezoelectric properties of the 0-3 PZT-Epoxy composites prepared [78], it was necessary to ensure that the there was no major differences between the particle size distribution and mean particle size of all the compositions of ceramic powders prepared. Table 4.1 shows the influence of Zr content on the particle size distribution (D10, D50 and D90) of the ceramic powder compositions. The standard deviation of the particle size was estimated to be 1.25 µm. Even though there is slight variation in the particle size distribution and mean particle size, the difference is not significant enough to have any influence on the dielectric and piezoelectric properties of the 0-3 PZT-Epoxy composites [79, 80].

Table 4.1: Particle Size Distribution of $PbNb_{0.01}[Zr_xTi_{(1-x)}]O_3$ ceramic powders for varying Zr mole%

Composition	D10 (µm)	D50 (µm)	D90 (µm)	Mean Particle Size (µm)
PT	0.65	1.35	3.40	1.70
PZT–10	1.19	2.92	3.74	2.33
PZT–20	0.79	2.22	4.24	2.40
PZT–30	0.64	1.97	5.02	2.53
PZT–40	0.92	2.26	4.69	2.60
PZT–45	0.92	2.15	4.11	2.56
PZT 50	0.67	2.21	4.84	2.50
PZT–52 (MPB)	0.68	1.92	4.35	2.57
PZT–60	0.73	2.41	5.43	2.95
PZT–70	0.77	2.59	5.45	3.05
PZT–80	0.74	2.49	5.48	3.076

4.1.4 Scanning Electron Microscopy (SEM)

The particle size and morphology of the $PbNb_{0.01}[Zr_xTi_{(1-x)}]O_3$ ceramic powders were analysed using scanning electron microscopy (SEM). Fig. 4.4 (a-c) shows the SEM micrographs of the calcined ceramic powder with Zr mole% corresponding to 0 (tetragonal), 0.52 (MPB) and 0.80 (rhombohedral) respectively. The particle size of the calcined powder was found to increase with Zr content, which was well supported by the results from particle size analysis of the ceramic powders compositions. The calcined PT powder appears to have spherical morphology whereas the other ceramic compositions possess polyhedral morphology.

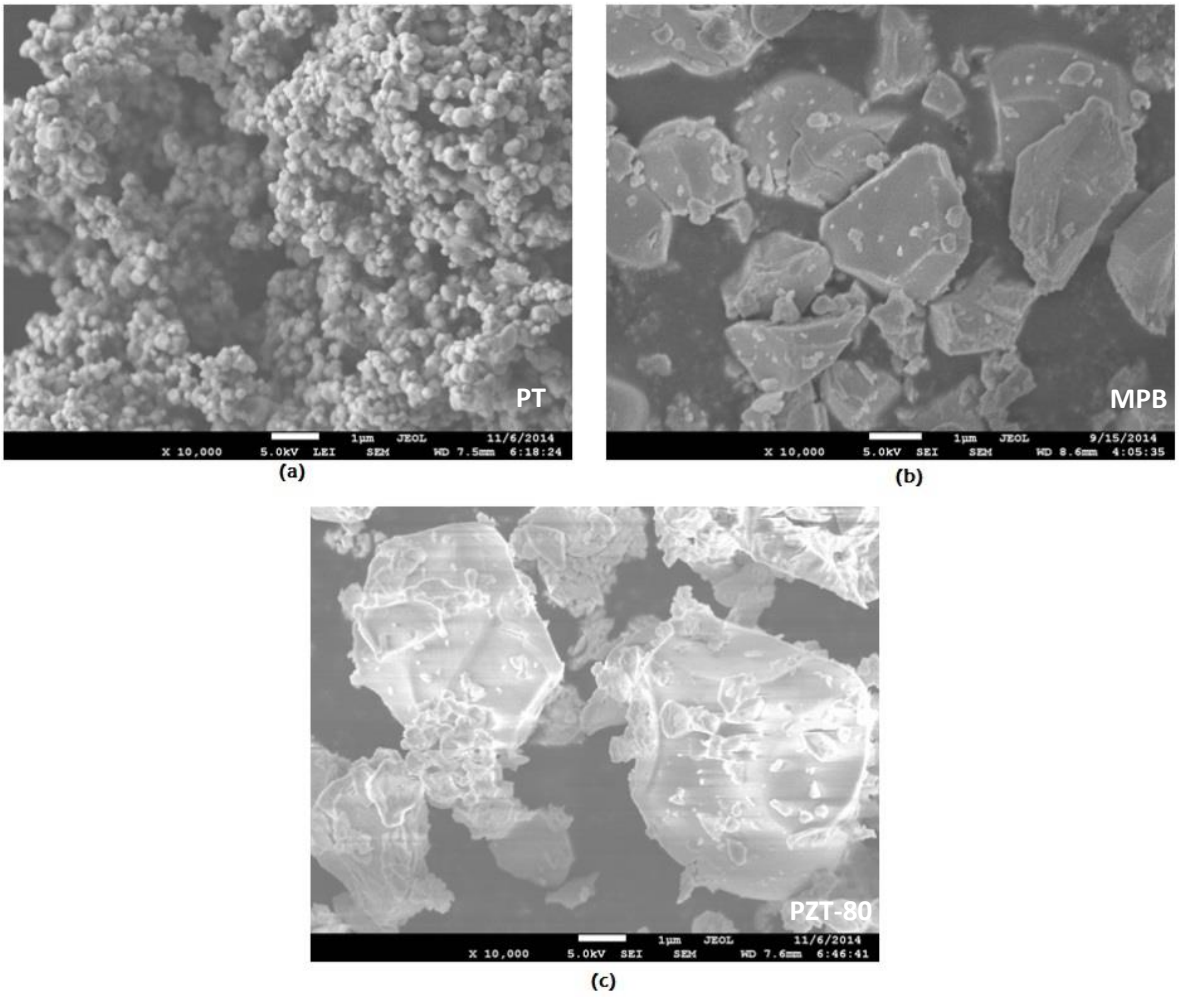

Fig. 4.4: Microstructure of ceramic powder for compositions corresponding to (a) PT, (b) MPB and (c) PZT-80 (i.e. *x* = 0.80)

Fig 4.5 (a-d) shows the SEM micrographs of ceramic disks sintered at 1250°C for Zr mole% corresponding to 0 (PT), 0.52 (MPB) and 0.80 respectively. It can be seen that the MPB and rhombohedral composition densely packed microstructure whereas PT has a porous microstructure, which shows the poor sinterability of tetragonal PZT ceramics. The reason

behind poor sinterability of PT ceramics is due to the large spontaneous strain and thermal expansion anisotropy of the tetragonal phase of lead titanate, which results in the mechanical fracture of the lead titanate ceramics (see Fig. 4.5(d)) as they are cooled from sintering temperature through the cubic to the tetragonal phase transition at 490°C [81]. In addition, the formation of pyrochlore phase is clearly observed in case of rhombohedral composition, which became less conspicuous with increasing Ti content in the ceramic powder compositions. The presence of non-ferroelectric pyrochlore phase will have a detrimental effect on the piezoelectric properties of the ceramics and thus need to be avoided [82]. But this formation of pyrochlore phase was not observed in case of calcined ceramic powder due to the two-stage calcination process followed (i.e. low temperature and high temperature calcination) [83].

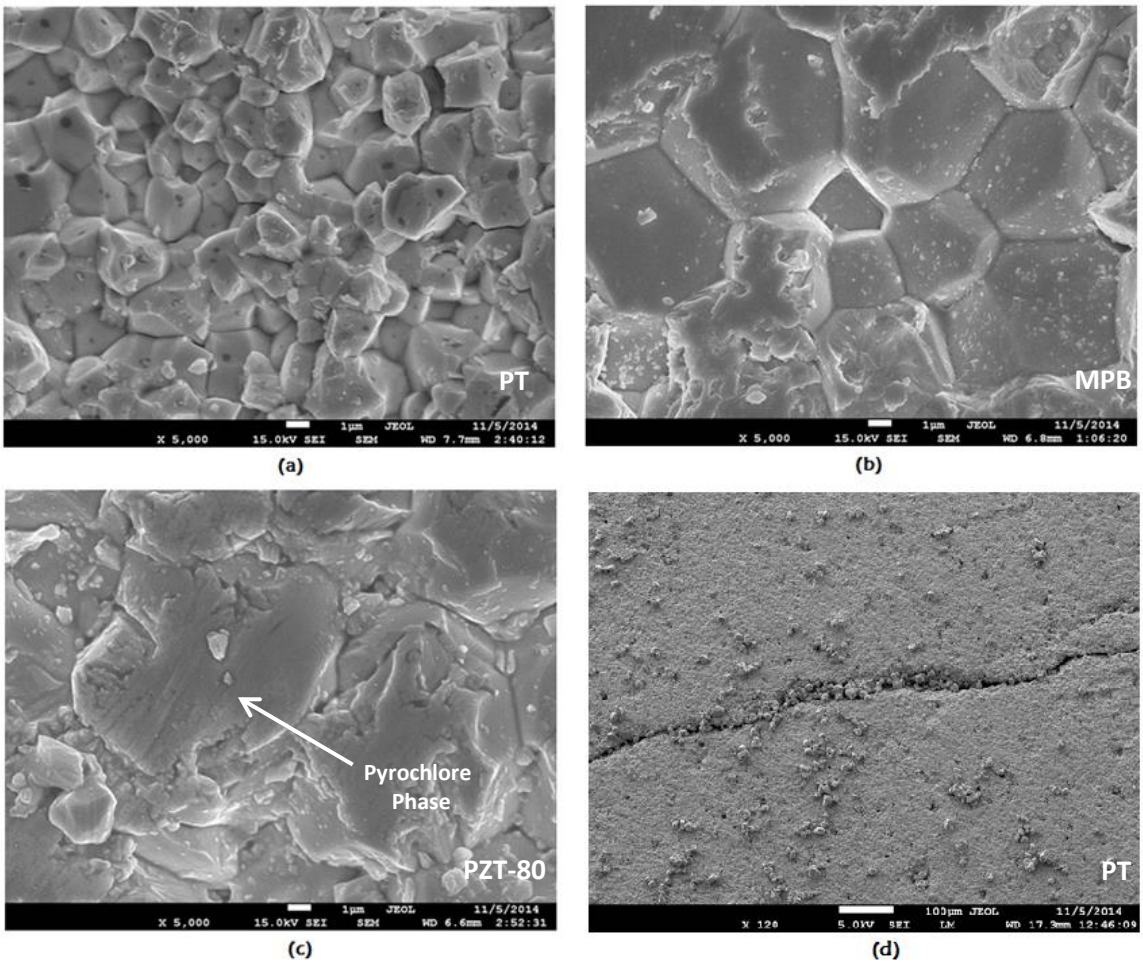

Fig. 4.5: Microstructure of ceramic disks sintered at 1250°C for compositions corresponding to (a) PT, (b) MPB, (c) PZT-80 (i.e. x = 0.80) and (d) crack on surface of PT ceramics after sintering process

The SEM micrographs were also used to analyse the dispersion of ceramic particles in the composites prepared. Fig. 4.6 shows the SEM micrographs of the cross-section of 0-3 PZT-

Epoxy Composites for 20 and 40 vol% of ceramic filler of PT and MPB composition. It can be seen that for 20 vol% composite, the system looks dilute with minimum particle to particle connectivity. On the other hand, in case of 40 vol% composite, a better particle to particle connectivity is observed, which results in higher piezoelectric properties with increasing volume percent of ceramic filler, as reported in prior works [41, 70].

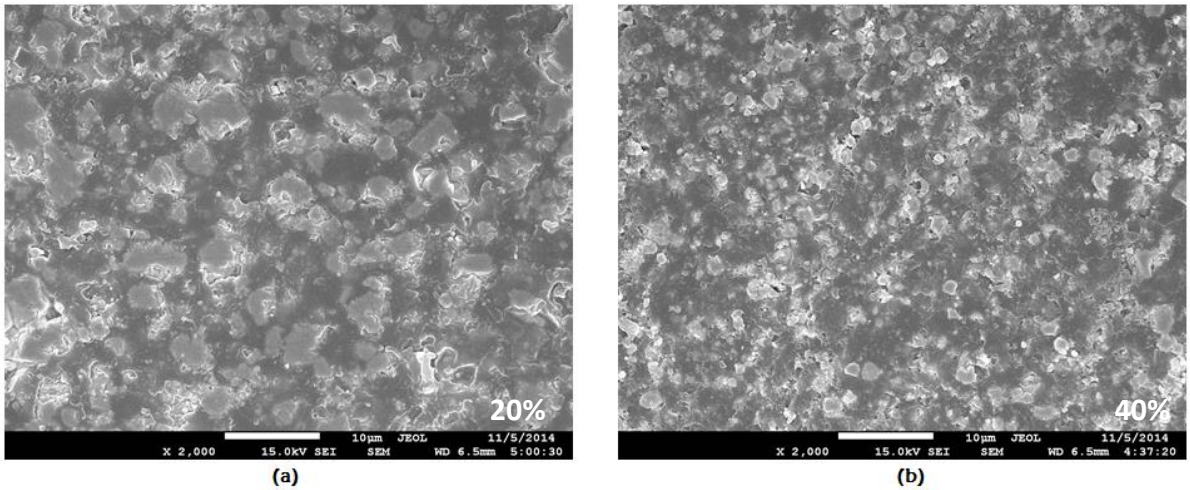

(a) (b)

Fig. 4.6: Cross-sectional micrographs of composites prepared with 20 vol% (a) and 40 vol% (b) of $PbNb_{0.01}[Zr_xTi_{(1-x)}]O_3$ ceramic powder with x = 0.52 (MPB)

4.2 Dielectric and Piezoelectric Properties

Table 4.2: Density of the sintered $PbNb_{0.01}(Zr_xTi_{(1-x)})O_3$ ceramics for x ranging from 0 to 0.80

Composition	Density (g/cm^3)
PT	7.12
PZT-10	7.18
PZT-20	7.20
PZT-30	7.25
PZT-40	7.30
PZT-45	7.35
PZT-50	7.41
PZT-52 (MPB)	7.49
PZT-60	7.41
PZT-70	7.41
PZT-80	7.39

Table 4.2 shows the densities of the sintered $PbNb_{0.01}(Zr_xTi_{(1-x)})O_3$ measured using the Archimedes method. The densities of the sintered ceramics are in the range of 7.12g/cm^3 to 7.49g/cm^3 (90-93 % of theoretical density) and are dependent on Zr composition. From the density values, it is evident that all the ceramic specimens prepared are eligible for electrical characterization.

4.2.1 Ceramics

Fig. 4.7 shows the electric-field induced polarization hysteresis of $PbNb_{0.01}(Zr_xTi_{(1-x)}))O_3$ ceramics, for x = 0, 0.52 (MPB) and 0.80, measured at an applied field ranging from 4.5 to 7.5 kV/mm and at room temperature. The hysteresis loop clearly shows that all the loops fully opened up and had attained polarisation saturation. The hysteresis measurement displays significantly higher remnant polarization (P_r) of MPB compositions than that of its tetragonal and rhombohedral compositions. The P_r increases with increasing Zr content upto MPB composition (x = 0.52) and then decreases. This behaviour is due the ferroelectric characteristics reaching its optimized values at MPB. However the decrease in P_r of PZT-80 composition is caused due to the Zr-rich rhombohedral phase in its composition [84].

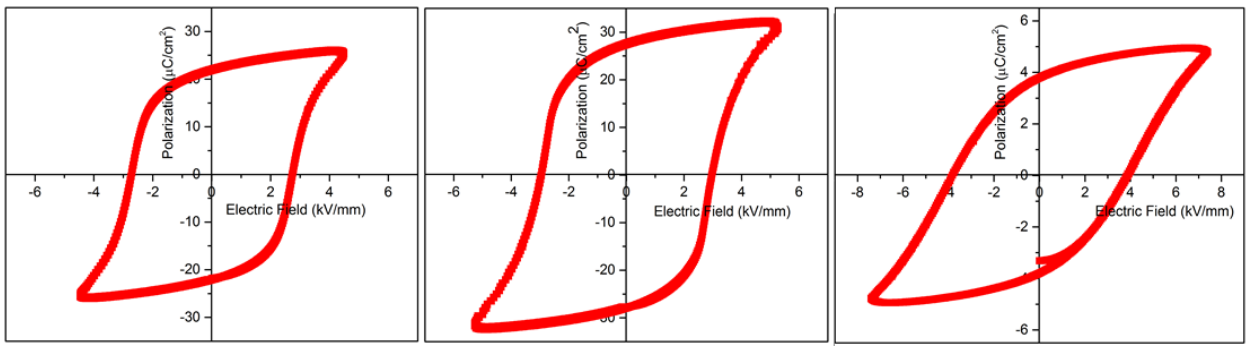

Fig. 4.7: P-E Hysteresis loop for $PbNb_{0.01}(Zr_xTi_{(1-x)})O_3$ ceramics for x = 0, 0.52 (MPB) and 0.80

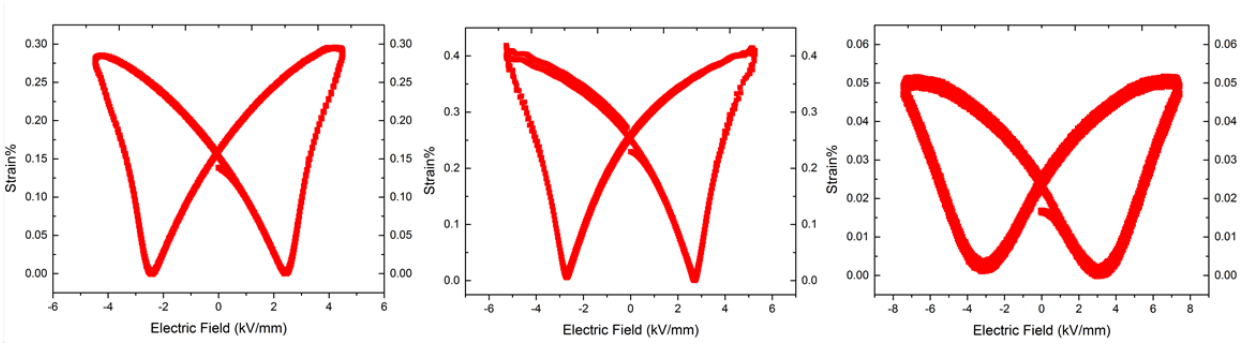

Fig. 4.8: The electric-field induced strain curves of $PbNb_{0.01}(Zr_xTi_{(1-x)})O_3$ ceramics, for x = 0, 0.52 (MPB) and 0.80

Fig. 4.8 shows the electric-field induced strain curves of $PbNb_{0.01}(Zr_xTi_{(1-x)})O_3$ ceramics, for x = 0, 0.52 (MPB) and 0.80, measured at a frequency of 1 kHz and at room temperature. It can be seen that each sample exhibits the classical butterfly shaped strain loops irrespective of their Zr composition. The well-defined strain loop of PT and MPB ceramics suggests that these ceramics possess excellent actuation properties compared to that of rhombohedral PZT ceramics. In general, the electric-field-induced strain in ceramics is caused by the complicated domain switching, piezoelectricity, electrostriction, and electric field. In other words, the strain value is dependent on the domain switching, piezoelectric constant, polarization, and applied electric field. As a result, MPB composition displays the maximum strain in ceramics due to the coexistence of rhombohedral and tetragonal phases at MPB, which in turn leads to enhanced polarization and piezoelectric properties [85].

Fig. 4.9 and 4.10 shows the variation of dielectric constant and piezoelectric charge constant of ceramics respectively, as a function of Zr composition. Since it is difficult to perform the poling process of tetragonal PZT ceramic, including PT, the piezoelectric charge constant (d_{33}) of the ceramics were determined by substituting the experimental values of the dielectric constant of corresponding composites in Eq. 1.18 from Yamada's model (See Fig. 4.9). The reason behind this difficulty in the poling process for tetragonal ceramic disks is due of the large coercive field of these ceramics [81]. In addition to this, as mentioned in Section 2.2, it was difficult to perform a complete sintering process of the tetragonal ceramics due to its large lattice anisotropy (*c*/a ratio for PT is 1.062) and high vapour pressure, thereby resulting in a fragile and porous ceramic disks .

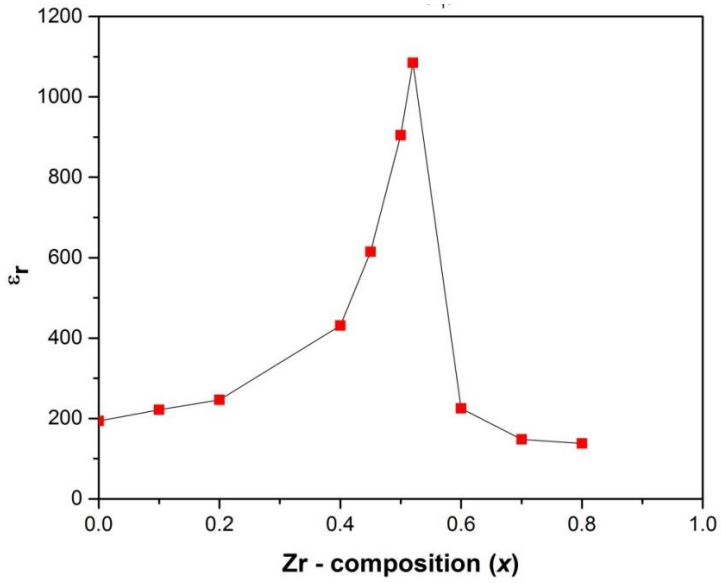

Fig. 4.9: Variation of room temperature dielectric constant (ε_r) of $PbNb_{0.01}[Zr_xTi_{(1-x)}]O_3$ as a function of Zr mole%

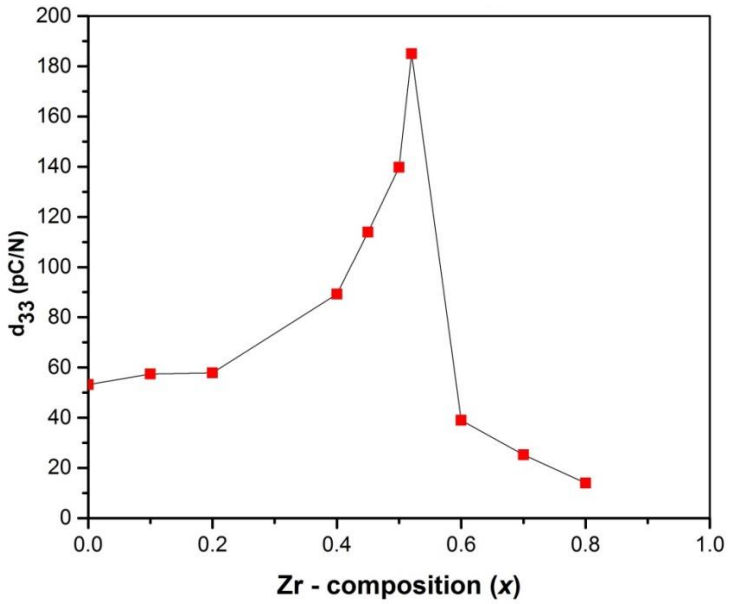

Fig. 4.10: Variation of room temperature piezoelectric charge constant (d_{33}) of $PbNb_{0.01}[Zr_xTi_{(1-x)}]O_3$ ceramics as a function of Zr mole%

Similar to dielectric constant, the maxima of the piezoelectric charge constant was also observed at MPB composition (See Fig. 4.10). The reason for this sharp increase in the dielectric and piezoelectric properties is attributed to the presence of 14 polarization directions, originating from the co-existence of tetragonal and rhombohedral phases at MPB, which are equivalent or nearly equivalent in free energy. This corresponds to highly polarizable state at MPB, which in turn favours strong dielectric and piezoelectric effects [5, 86, 87]. As mentioned previously, when $x > 0.52$, the composition has only rhombohedral phase whereas when $x < 0.52$, the composition is dominated by tetragonal phase. In either case, the number of domain variants is less than that of MPB composition, which in turn inhibits the piezoelectric response of the ceramics. In addition, the porous nature of tetragonal ceramic disks also contributed towards the decrease in piezoelectric charge constant since the presence of pores reduces the polarization per unit volume [5, 88] , which in turn reduces d_{33}.

4.2.2 Composites

The electric-field dependence of polarization studies for 0-3 composites were carried out for different applied fields (5 – 40 kV/mm) at room temperature and the loops are shown in Fig. 4.11. The development of hysteresis loop confirms the ferroelectric nature of the 0-3 PZT-Epoxy composites prepared. With the increase in the electric field, the composites exhibited higher polarization due to the alignment of the dipoles within the material, resulting in an increase in the area of the P-E loops. However, the remnant polarization (P_r) is much lower than that of bulk ceramics due to the influence of the non-ferroelectric polymer phase. It can also be seen that the poling efficiency of composites with 40 vol% of ceramic filler is much higher than

that of the ones with 20 vol%. This is due to the better connectivity of the ceramic filler particles in the composites with 40 vol% of ceramic filler.

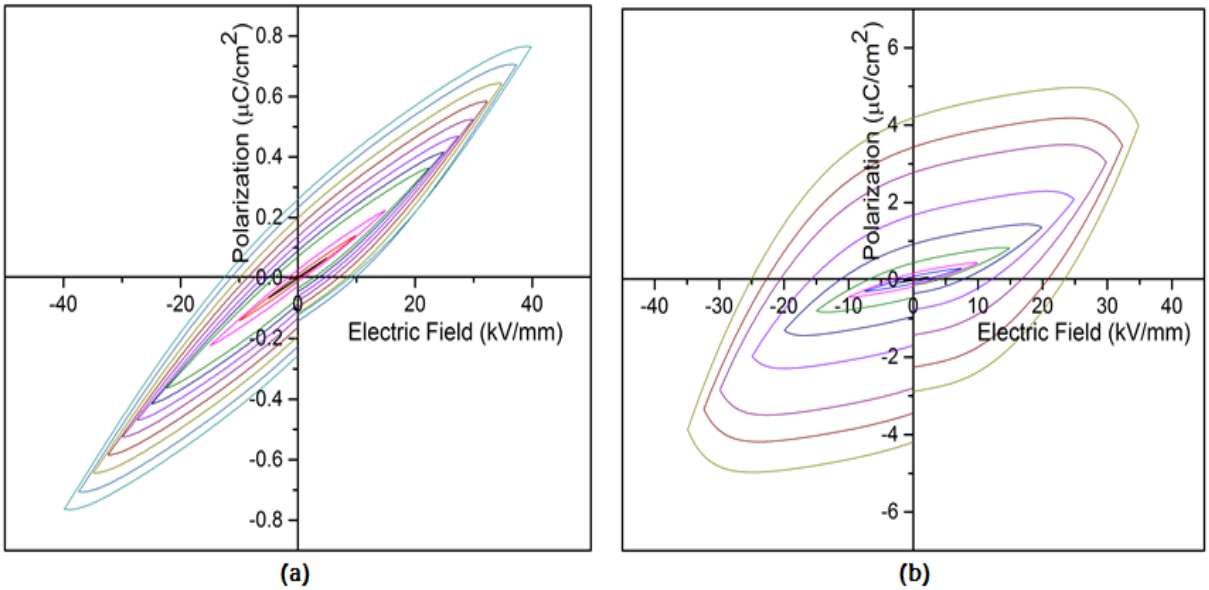

Fig. 4.11: Polarization hysteresis loop for (a) 20 vol% and (b) 40 vol% of 0-3 PZT (MPB)-Epoxy Composite

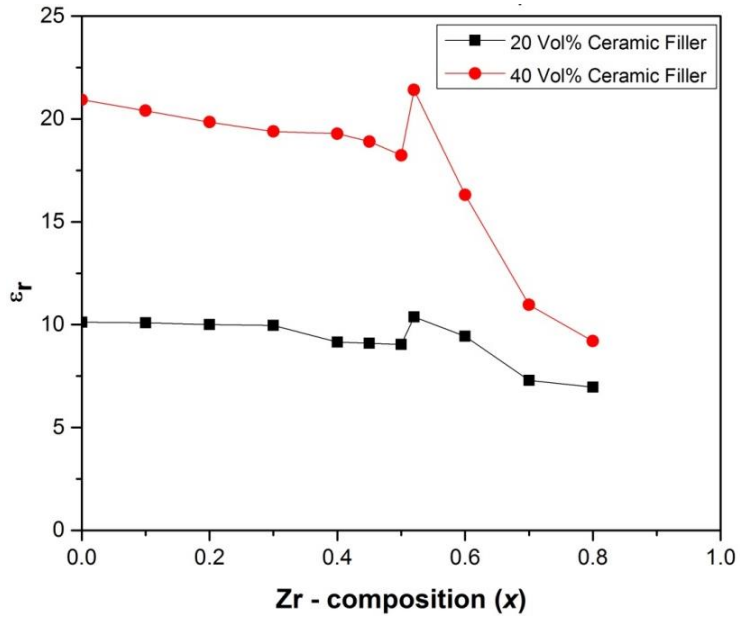

Fig. 4.12: Dielectric Constant (ε_r) as a function of Zr mole% in 0-3 Composites with 20 and 40 vol% of $PbNb_{0.01}[Zr_xTi_{(1-x)}]O_3$ ceramic filler

Fig. 4.12 shows the variation of dielectric constant of 0-3 PZT-Epoxy composites as a function of Zr composition. Compared to that of bulk ceramics (Fig. 4.8), the lower dielectric constant observed in composites is due to the presence of passive polymer phase surrounding the active ceramic phase within the 0-3 PZT-Epoxy composite. It is also noteworthy that even though there is a large difference between dielectric constant of PT and MPB ceramics, when

these ceramics compositions are used as a filler material in composites, the effective dielectric constant of the composite do not exhibit such a significant difference. Another major observation is the relatively lower difference between the dielectric constants of PT and MPB composites compared to that of its corresponding bulk ceramics. From Fig. 4.9, it can be seen that the difference between the dielectric constant of PT and MPB ceramic disks is about 885 whereas in case of 0-3 composites, this difference has drastically reduced and both the composites possess about same dielectric constant. As a result, it could be seen that even after the addition of ceramic fillers with a wide range of dielectric constant, the resultant dielectric constant of the composites remains within smaller range. The reason behind this anomaly between bulk ceramics and composites is related to the difference in the dielectric constant of each constituent (i.e. PZT ceramic filler and epoxy matrix) [89]. Considering 0-3 composite, which contains ceramic powder with MPB composition as filler, the difference in the dielectric constant of epoxy matrix ($\varepsilon_{r,\ epoxy}$ = 4.2) and the ceramic filler ($\varepsilon_{r,\ filler}$ = 1085) is about 1081. Alternatively, in case of PT ceramic filler ($\varepsilon_{r,\ filler}$ = 200), the difference is only 196. This lower difference between the dielectric constant of the polymer and ceramic phase has resulted in a better homogenization between the PT ceramic filler and epoxy matrix in 0-3 composites and thus had resulted in a dielectric constant, which is comparable to that of MPB composites. This observation is well supported by the results obtained by the experimental analysis and analytical models as shown in Fig. 4.13 and 4.14. It is clearly evident that, in all analytical models, the dielectric constant of composites attains saturation after a sharp increase with the dielectric constant of constituent ceramic fillers in the initial stage. Once saturated, the increase in the dielectric constant of ceramic filler particles does not have any significant impact on the dielectric constant of its composites. This observation is consistent with the experimental results also.

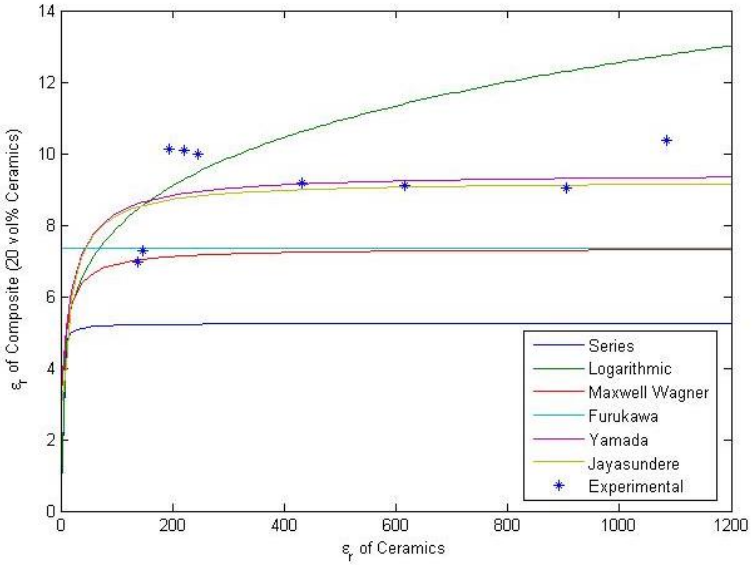

Fig. 4.13: Variation of dielectric constant of 0-3 composite (20 vol%) as a function of the dielectric constant of corresponding $PbNb_{0.01}[Zr_xTi_{(1-x)}]O_3$ ceramic compositions - Experiemental v/s Analytical

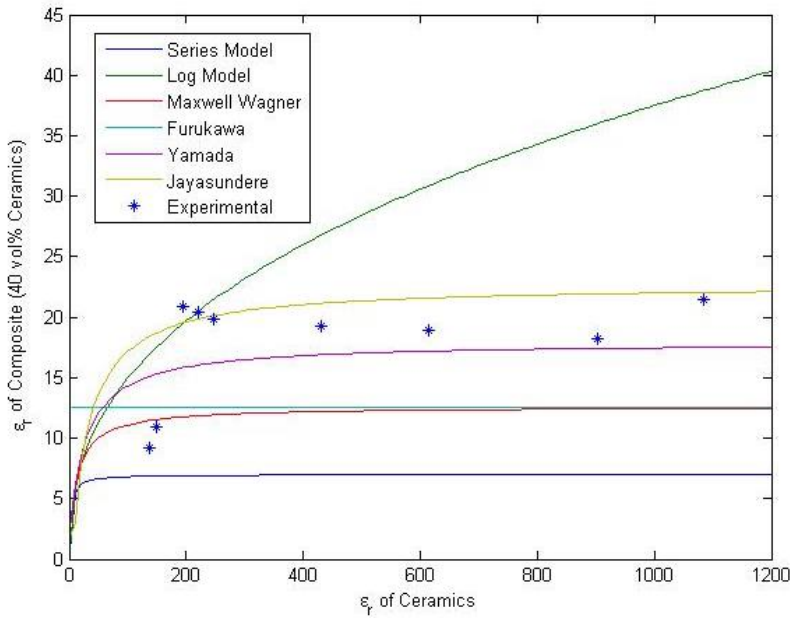

Fig. 4.14: Variation of dielectric constant of 0-3 composite (40 vol%) as a function of the dielectric constant of corresponding $PbNb_{0.01}[Zr_xTi_{(1-x)}]O_3$ ceramic disks - Experiemental v/s Analytical

Fig. 4.15 shows the variation of piezoelectric charge constant (d_{33}) as a function of Zr mole% for 0-3 PZT-Epoxy composites. As evidenced by prior works [30, 40], composites with 40 vol% of ceramic filler show higher d_{33} than those with 20 vol% of filler due to the presence of higher content of active ceramic phase and better connectivity between the ceramic filler particles. Similar to that of bulk PZT ceramics reported by Jaffe, an increase in the d33 of composites is observed, with the increasing Zr content, for compositions close to MPB (i.e. from x=0.5), attaining its maxima at x=0.52 (i.e. MPB composition). This is due to the higher poling efficiency of the PZT ceramics at MPB composition. . On further addition of Zr content (i.e. x > 0.52), the antiferroelectric rhombohedral phase dominates, resulting a sharp decline in the d33 of ceramic filler and consequently its composites. Another striking feature observed is the relatively higher d_{33} of 0-3 composites with PT (x = 0) ceramic fillers compared to that of the one with MPB (x = 0.52) ceramic filler. Fig. 4.16 and 4.17 shows the results of the analytical models used to predict the d_{33} of composites (20 and 40 vol% of ceramic fillers respectively) as a function of ε_r of ceramic fillers used. Similar to the observation made in case of effective dielectric constant of composites, the d_{33} of the composites also attained saturation after a sharp increase with the dielectric constant of constituent ceramic fillers in the initial stage. Once saturated, the increase in the dielectric constant of ceramic filler particles does not have any significant impact on the dielectric constant of its composites. The phenomenon which is responsible for this observation is known as the depolarization effect (shown in Fig. 4.20), which will be discussed in detail in Section 4.5.

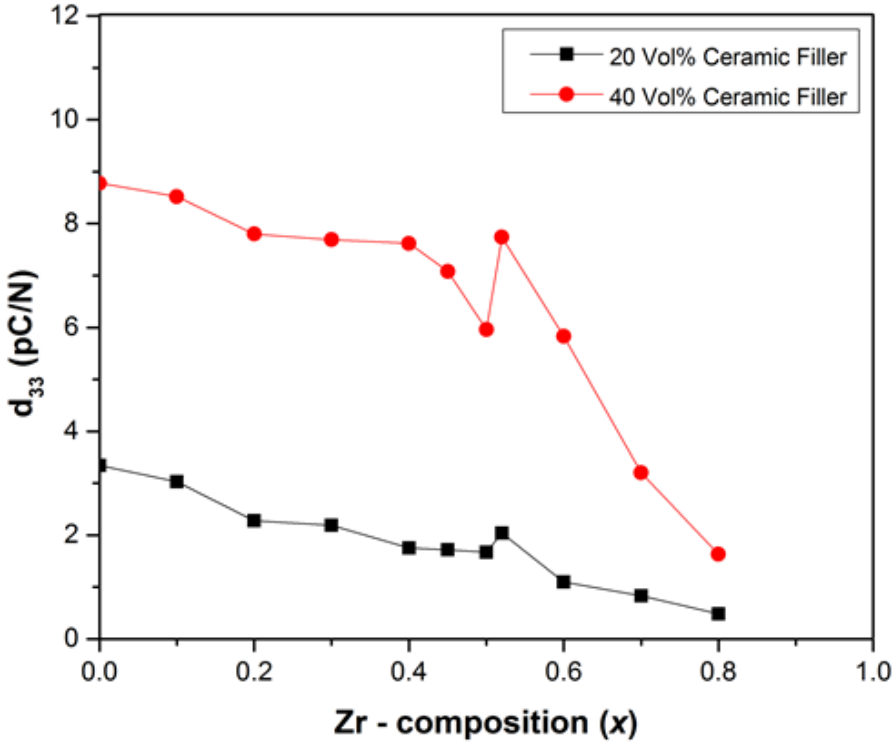

Fig. 4.15: Variation of room temperature piezoelectric charge coefficient (d_{33}) of 0-3 Composites for 20 and 40 vol% of $PbNb_{0.01}[Zr_xTi_{(1-x)}]O_3$ ceramic filler

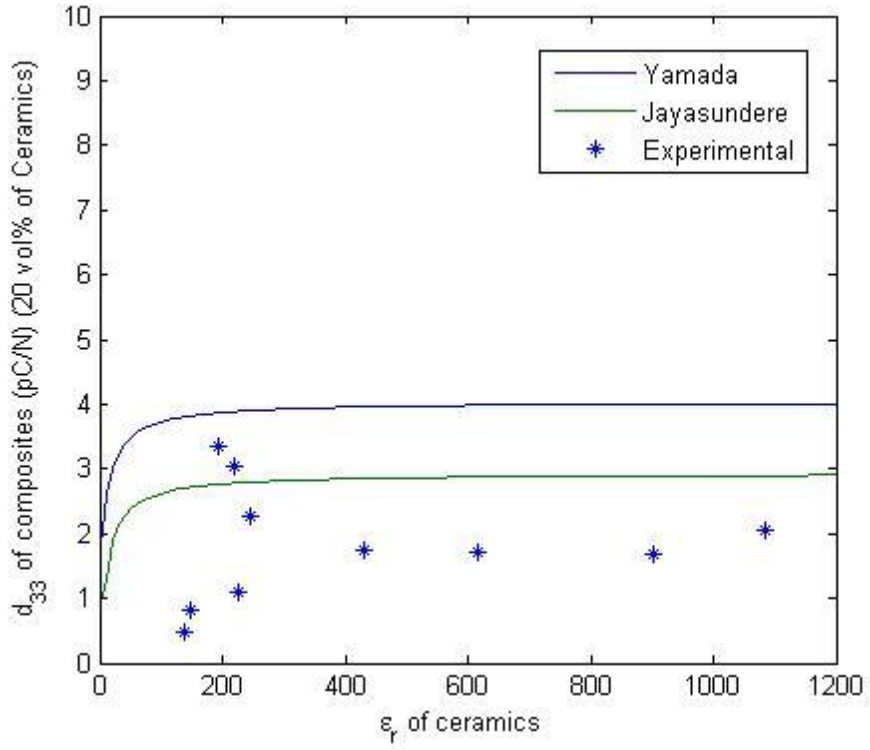

Fig. 4.16: Variation of room temperature piezoelectric charge constant (d_{33}) of 0-3 Composites for 20 vol% of $PbNb_{0.01}[Zr_xTi_{(1-x)}]O_3$ ceramic filler

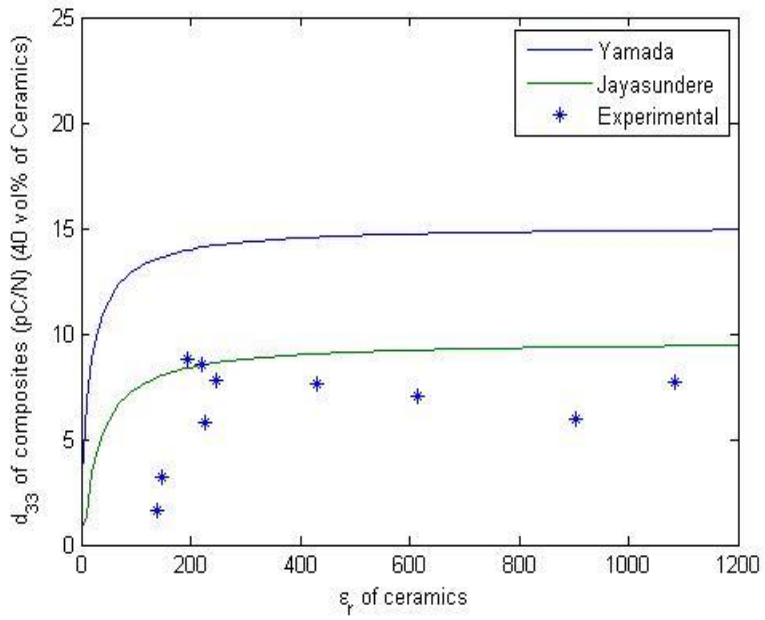

Fig. 4.17: Variation of room temperature piezoelectric charge constant (d_{33}) of 0-3 Composites for 40 vol% of $PbNb_{0.01}[Zr_xTi_{(1-x)}]O_3$ ceramic filler

4.3 Voltage Sensitivity

4.3.1 Ceramics

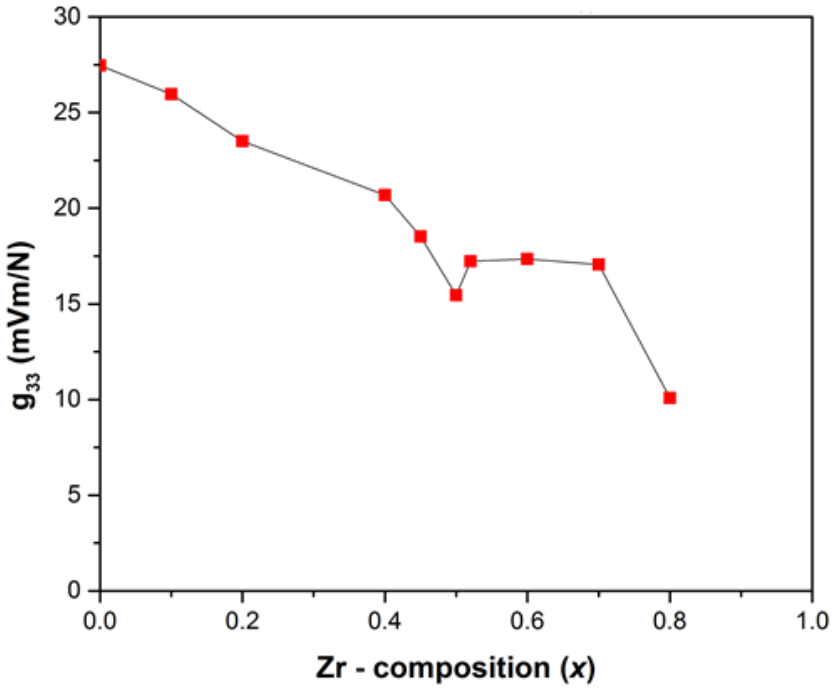

Fig. 4.18: Variation of room temperature piezoelectric voltage coefficient (g_{33}) of $PbNb_{0.01}[Zr_xTi_{(1-x)}]O_3$ ceramics

The piezoelectric voltage coefficient (g_{33}), shown in Fig. 4.18 was calculated using Eq. 1.6, which was presented in Section 1.4.3. It can be seen that the highest g_{33} is exhibited by $PbTiO_3$ (PT) ceramics, in spite of its lower d_{33} than that of MPB ceramics. The reason behind this anomaly is the significantly lower dielectric constant of PT (ε_r = 194) compared to that of MPB ceramics (ε_r = 1085). It is noteworthy that the piezoelectric voltage coefficients (g_{33}) increases towards the tetragonal field while it remains almost constant in the rhombohedral field until the antiferroelectric nature of the rhombohedral phase gains over the ferroelectric properties, after which the g_{33} drops down significantly.

4.3.2 Composites

The piezoelectric voltage constant (g_{33}) as a function of Zr composition is shown in Fig. 4.19. Similar to that of ceramics, the g_{33} values of the composites were also obtained using the Eq. 1.6 and it ranges from 11 to 42 mV.m/N, depending upon the vol% of ceramic filler and Zr mole%. The highest value of 42 mV.m/N for composite with 40 vol% of PT ceramic filler was found to be comparable with the values reported previously [90]. The reason behind the highest voltage sensitivity of PT composites can be attributed to the moderately high d_{33} and relatively lower dielectric constant of 0-3 PT-Epoxy composites compared to that of its MPB counterpart (see Fig 4.12 and 4.15). This high g_{33} value makes the 0-3 PT-Epoxy composite a very attractive material for sensory applications.

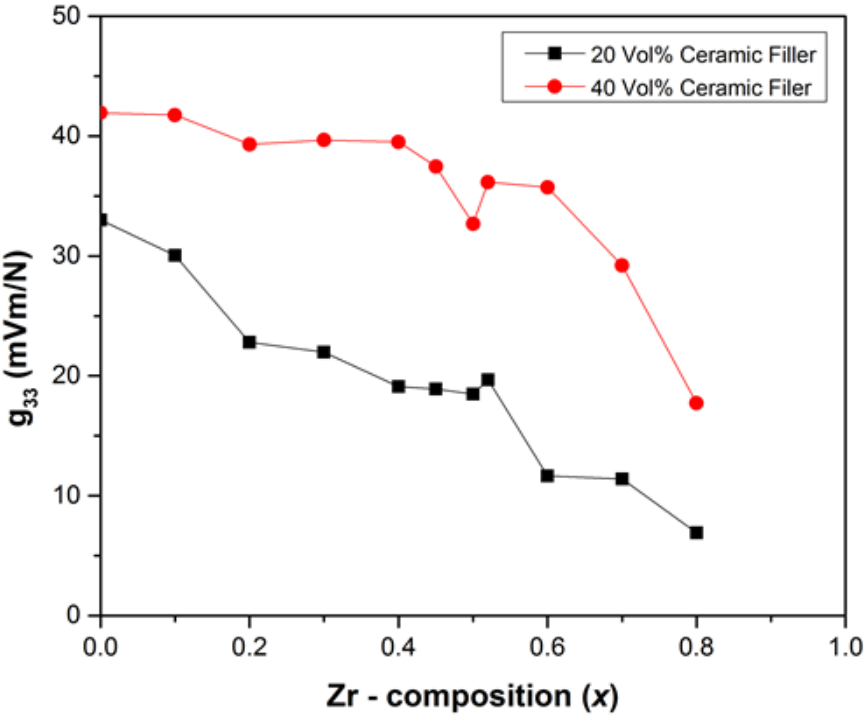

Fig. 4.19: Variation of room temperature piezoelectric voltage coefficient (g_{33}) of 0-3 Composites for 20 and 40 vol% of $PbNb_{0.01}[Zr_xTi_{(1-x)}]O_3$ ceramic filler

4.4 Comparison of Dielectric and Piezoelectric Properties – Sintered ceramics and composites

As mentioned in earlier sections, most of the prior works on piezoelectric materials involves the application of MPB or close to MPB compositions of PZT ceramics due to the enhanced dielectric and piezoelectric properties observed at MPB. This is also evident from Fig. 1.8 – 1.10, reported by Jaffe et al. Since the current work explored the entire range of PZT phase diagrams and systematically studied the dielectric and piezoelectric properties of ceramic compositions corresponding to $PbNb_{0.01}(Zr_xTi_{(1-x)})O_3$, ranging from pure tetragonal (x = 0) to rhombohedral (x = 0.80) ceramics. The dielectric and piezoelectric properties of sintered ceramics prepared from these compositions, shown in Fig 4.8 and 4.9, clearly displays the highest piezoelectric and dielectric properties at of MPB compositions. As far as voltage sensitivity of the sintered ceramics are considered, it can be seen that PT and MPB based ceramics have comparable g_{33} but the poor sinterability and poling difficulties associated with PT ceramics restricted its application in piezo devices.

In case of composites, in spite of having observed a significant increase in the ε_r and g_{33} of MPB based composites, shown in Fig. 4.12 and 4.15, the difference between the dielectric and piezoelectric properties of MPB and non-MPB based composites were not as significant as their sintered ceramics as shown in Fig. 4.9 and 4.10. Due to this unique combination of lower dielectric constant and moderately higher d_{33}, composites with PT ceramic fillers exhibited a higher g_{33} than that of its MPB and close to MPB counterparts (see Fig. 4.19). In addition, the poor sinterability associated with sintered ceramics was not an area of concern in case of composites, since the composites made of calcined ceramic filler particles. As a result, the PT based composite materials can be considered as an excellent candidate towards piezoelectric sensor devices.

4.5 Depolarization Field

When a dielectric material, such as the ceramic filler, is polarized under an applied electric field, surface charges appears along the boundaries of each of the ceramic particles embedded in the polymer matrix (shown in Fig. 4.20). The formation of these surface charges results in the production of a depolarization field (E_D) that acts opposite to the applied electric field (E_0). As a result, the net polarization within the caramic particle gets deteriorated while the field outside remains the same [91]. In addition, the magnitude of depolarization field increases with increasing dielectric constant of the particle. Hence, by comparing the above mentioned relation between deplorization field and dielectric constant of ceramics (Fig. 4.9), it can be concluded that the increase in the d_{33} in 0-3 composites with decreasing Zr content is due to the

corresponding decrease in the dielectric constant of the ceramics. This has resulted in higher d_{33} for PT composites compared to that of its MPB counterpart. Eq. 4.1 and 4.2 shows the expression for depolarization factor (α) and effective dielectric constant of composites (ε_c) respectively. The model consists of a filler material with dielectric constant ε_f (i.e. ceramics) embedded as spheres in a matrix with dielectric constant ε_f (i.e. polymer). The parameter V corresponds to the total volume of filler material in a sphere and is given by $V = V_f/N$, where V_f is the volume fraction of filler material and N is interpreted as the number of spheres per unit volume.

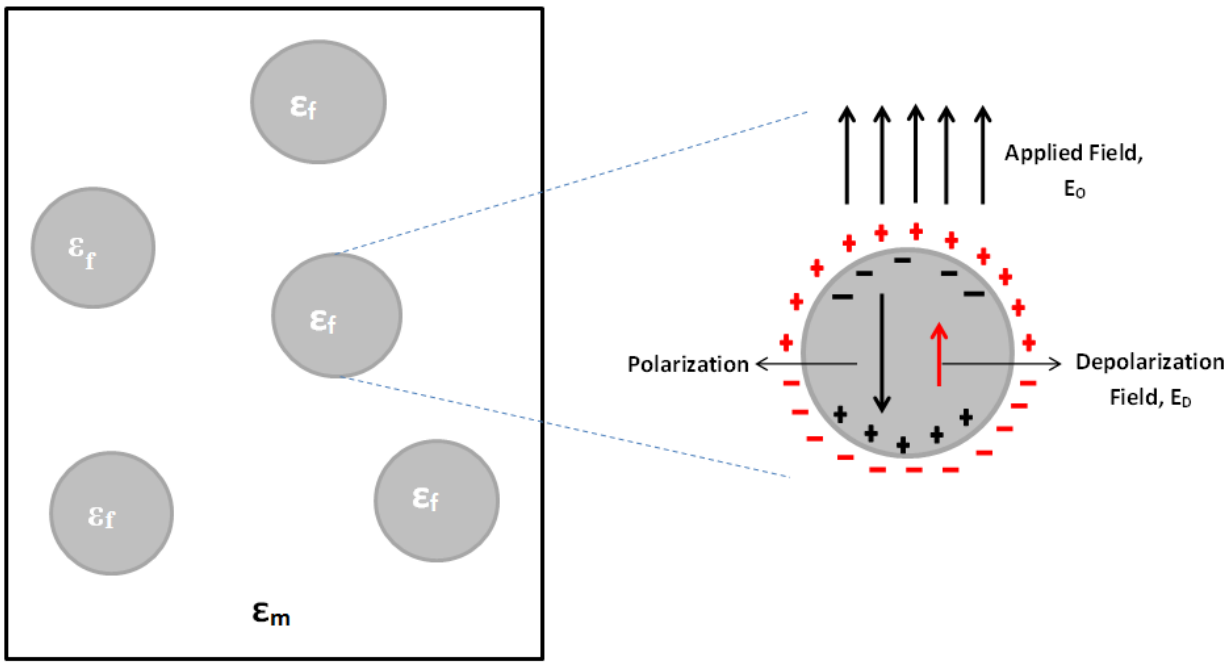

Fig. 4.20: Depolarization Effect [91]

$$\alpha = \frac{3\varepsilon_m(\varepsilon_f - \varepsilon_m)}{(\varepsilon_f + 2\varepsilon_m)}V \qquad (4.1)$$

$$\varepsilon_c = \varepsilon_m \left(\frac{1 + \frac{2N\alpha}{3\varepsilon_m}}{1 - \frac{N\alpha}{3\varepsilon_m}} \right) \qquad (4.2)$$

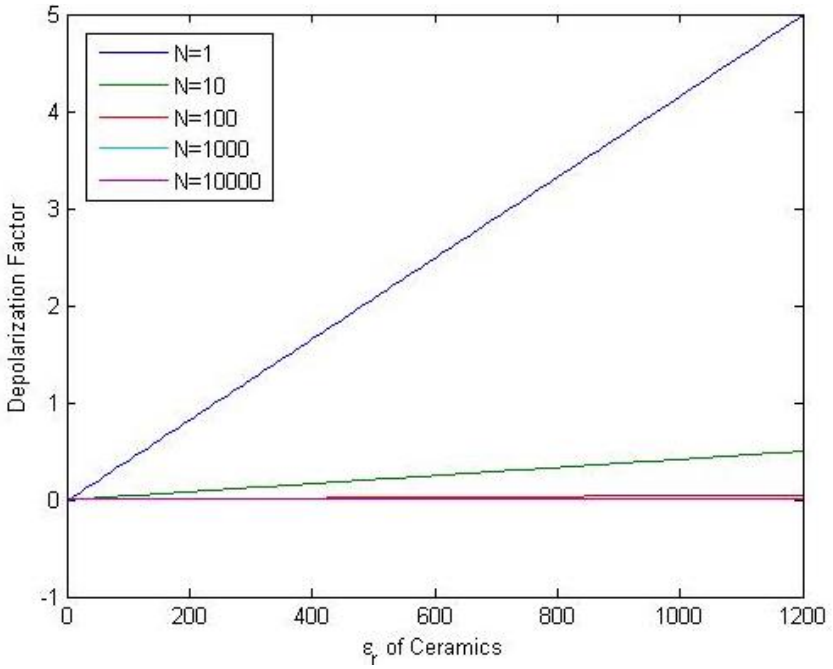

Fig. 4.21: Depolarization factor as a function of dielectric constant of the ceramic inclusions for different N values

Fig. 4.21 shows depolarization factor as a function of dielectric constant of the ceramic inclusions for different N values. The value of N corresponds to the number of particles within the polymer medium. It could be seen that the depolarization factor increases with increasing ε_r of the ceramic filler and this dependence is the driving force behind the observed trend in the experimentally determined ε_r and d_{33} of composites. In addition to this, it could also be seen that the effect of depolarization factor got drastically reduced with increase in number of particles. The reason behind this significant reduction can be attributed towards the better connectivity between the ceramic filler particles with increase in N value

4.6 Polarization Fatigue

The effect of electric field on the remnanat polarization of PT and MPB composites over a period of 10^5 cycles at room temperature are shown in Fig 4.22. It is observed that the MPB composites undergoes a wide range of variation in its polarization during the the electric cycles where as in case of PT composites, the electric field have relatively less impact on polarization. This decrease in polarization of MPB composites will have a detrimental effect on the sensorial properties of the composites. It is most likely that such a drop in polariation and thereby sensorial properties, is caused by the delamination between PZT filler particles and the polymer matrix since no intrinsic changes in the properties of the constituent ceramic and polymer phases are to be expected at room temperature. Thus, 0-3 composites with PT ceramic filler exhibits greater resistance to electric fatigue that its MPB counterpart over a longe range of electric cycles.

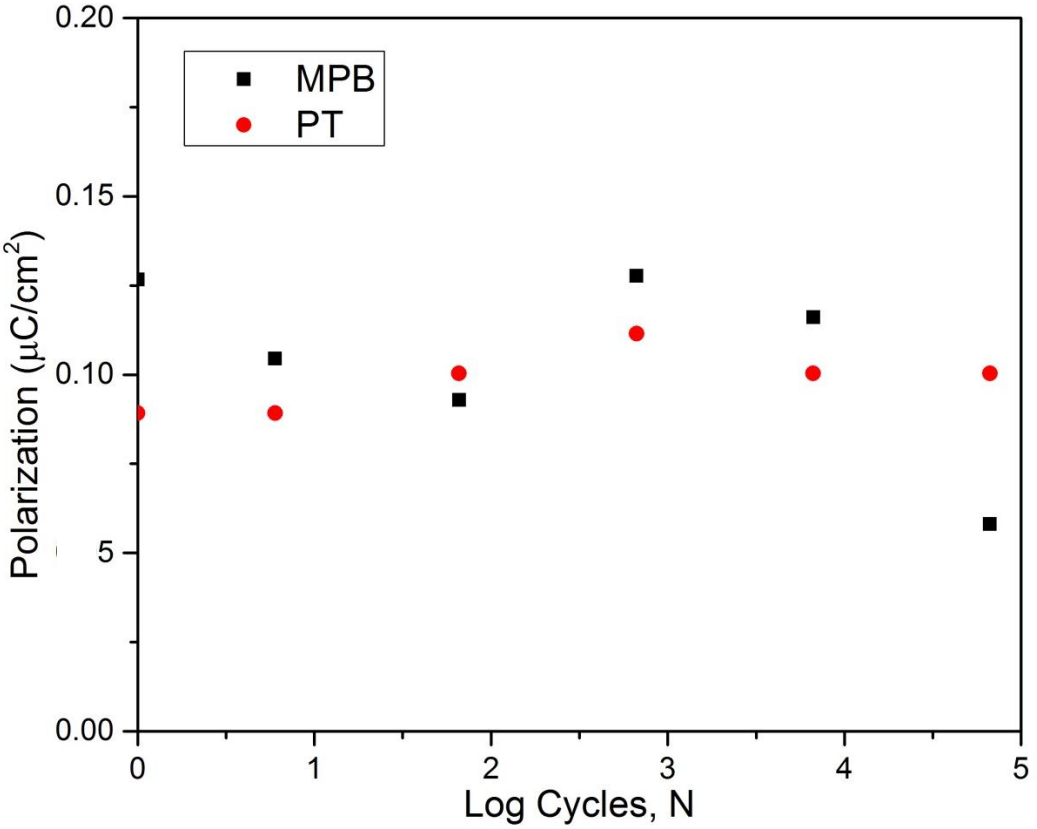

Fig. 4.22: Polarization fatigue of 0-3 composites with 40 vol% of PT and MPB based ceramic filler

5. Conclusions and Recommendations

5.1 Conclusions

In the present work, the whole range of PZT compositions, having the general formula $PbNb_{0.01}(Zr_xTi_{(1-x)})O_3$ (for x=0 to 0.8), and its corresponding sintered ceramics and composites were prepared and studied. The PZT compositions were prepared by means of conventional mixed oxide methods, during which a two-stage calcination process was adopted in order to obtain pure perovskite structure. The formation of the perovskite structure and phase transformation, due to varying Zr/Ti ratio, was confirmed using X-ray Diffraction (XRD) analysis of the ceramic powders prepared. The XRD results revealed the co-existence of rhombohedral and tetragonal phases at Zr/Ti ratio of 52/48 (MPB). The XRD results were also used to determine the lattice parameters of the ceramic powder compositions, which further confirmed the phase transformation from rhombohedral to tetragonal with decreasing Zr/Ti ratio. The microstructure and particle size distribution of the ceramic particles were analysed using scanning electron microscope (SEM) and laser diffractometry respectively. The laser diffractometry results confirmed that the particle size distribution of the ceramic powders prepared were within 2 – 3 μm. The calcined PZT powder compositions were sintered and pressed into ceramic disks and was also used as ceramic filler materials to prepare 0-3 piezoelectric composites. The piezoelectric behaviour of the sintered ceramics and 0-3 composites were studied using polarization hysteresis (P-E) and strain loop measurement. The effect of Zr/Ti ratio on the dielectric and piezoelectric properties of both MPB and non-MPB compositions in ceramics and composites were studied. Finally, the influence of electric fatigue on the polarization of the $PbTiO_3$ (PT) and morphotropic phase boundary (MPB) based composites were analysed.

The P-E measurement of sintered ceramics showed saturated loops with remnant polarization ranging from 4 to 28 $\mu C/cm^2$ depending upon the Zr composition. On the other hand, the P-E hysteresis measurement of 0-3 composites exhibited unsaturated and closed loops even at a very high applied field. This is due to the presence of polymer phase, which obscures a major part of the applied electric field. The dielectric and piezoelectric properties of the sintered ceramics and composites were measured and validated using several existing analytical models. The results of dielectric measurement showed that even though there is a

large difference between the dielectric constant (ε_r) of PT and MPB based ceramics, when these ceramic compositions are used as fillers in composites, the effective ε_r of the composites does not exhibit such a significant difference. The reason behind this anomaly is attributed towards the non-homogeneity between the dielectric constant of the ceramic filler particles and polymer matrix. This non-homogeneity, results in the formation of an electric field within the ceramic filler particle, which tends to oppose the applied electric field. This phenomenon, known as depolarization effect, comes into play due to the dispersion of highly dielectric PZT ceramic fillers (ε_r = 1080) particles in a lower dielectric epoxy matrix (ε_r = 4.8). The extent of depolarization field is directly proportional to ε_r of the ceramic filler and thus higher the ε_r of the ceramic filler, higher will be the depolarization field, which in turn has a detrimental effect on the effective ε_r of the composite. Since both, dielectric and piezoelectric charge constants (d_{33}) are the measure of polarizability of a piezoelectric materials, the same depolarization effect is the reason behind the relatively higher effective d_{33} of PT composites. This lower ε_r combined with relatively higher d_{33} had led to a reasonably higher piezoelectric voltage coefficient (g_{33}) in PT composites compared to that of MPB composites.

As a result, this combination of low dielectric constant and moderately high piezoelectric charge constant (d_{33}) characterizes the 0-3 PT-Epoxy composites as excellent materials for voltage sensitivity. Hence, in a nutshell, this entire research work successfully explored the possibility of using non-MPB ceramic compositions in 0-3 composites for sensoric applications.

5.2 Recommendations

A knowledge base of dielectric and piezoelectric properties of 0-3 PZT-Epoxy composites based on the entire PZT phase diagram and ceramic filler material selection criteria has been established and documented in this research work. The findings of this research work will serve as a basis for further research into non-MPB based piezoelectric ceramic – polymer composites and a detailed research must be conducted for a thorough understanding on material and processing properties in order to optimize the dielectric and piezoelectric properties of the composite. Considering the outcome of the current research, following recommendations can be formulated for further research on this topic.

I. Lead free replacement of PZT powder:
   Due to the health hazards posed by lead, the PZT ceramic powder can be replaced with lead-free ceramics materials such as $BaTiO_3$, KNN and BNT-BT. This replacement will result in the fabrication of environmental friendly piezoelectric-polymer sensory composites.

II. Improved composite manufacturing techniques:

Apart from tape-casting, the piezoelectric composites could also be prepared through various other techniques such as by hot press and solvent casting. This would enable to compare the difference in the dispersion of ceramic filler particles and density of the composites, which in turn would have an impact on the dielectric and piezoelectric properties of the final composite. In addition, 0-3 piezoelectric composites can be by the process of dielectrophoresis (DEP), which has already been proved as a reliable technique to enhance the dielectric and piezoelectric properties of the 0-3 piezoelectric composites by converting them to quasi 1-3 composites. The same DEP can be used in case of non-MPB based composites, especially PT composites, in order to further enhance their ε_r and d_{33} and thereby resulting in a higher g_{33} or voltage sensitivity.

III. Influence of different matrix types:

The effect of a different matrix type on the dielectric and piezoelectric properties of the composite could be studied further since matrices with higher ε_r could have a great influence on the properties of the composite. The increase in piezoelectric properties could even lead to the development of good piezoelectric composites sensors with lower volume percent ceramic fillers, which in turn results in more flexible composites.

IV. Potential applications in the field of aerospace engineering:

Since the non-MPB based composites has been proved to have higher voltage sensitivity, further works could be initiated in stretching out the potential applications of these composites in smart materials and structures for energy harvesting, structural health monitoring and vibrational dampeners.

References

[1] B. Jaffe, W. R. Cook Jr, and H. Jaffe, *Piezoelectric ceramics* vol. 3: Elsevier, 2012.

[2] S. Saadon and O. Sidek, "A review of vibration-based MEMS piezoelectric energy harvesters," *Energy Conversion and Management,* vol. 52, pp. 500-504, 2011.

[3] J. F. Tressler, S. Alkoy, and R. E. Newnham, "Piezoelectric sensors and sensor materials," *Journal of Electroceramics,* vol. 2, pp. 257-272, 1998.

[4] "Piezoelectric Ceramics: Electro Ceramic Solutions," *Morgan Advanced Materials (www. moganadvancedmaterials.com)*.

[5] J. Holterman and P. Groen, *Piezoelectric Materials and Applications*. Apeldoorn (the Netherlands): Stichting Applied Piezo, 2012.

[6] A. Vázquez Carazo, "Novel piezoelectric transducers for high voltage measurements," 2000.

[7] K. Uchino, *Advanced piezoelectric materials: Science and technology*: Elsevier, 2010.

[8] S. R. Moheimani and A. J. Fleming, *Piezoelectric transducers for vibration control and damping*: Springer, 2006.

[9] A. Meitzler, H. Tiersten, A. Warner, D. Berlincourt, G. Couqin, and F. Welsh III, "IEEE standard on piezoelectricity," ed: Society, 1988.

[10] S. J. Yoon, H. W. Kang, S. I. Kucheiko, H. J. Kim, H. J. Jung, D. K. Lee, and H. K. Ahn, "Piezoelectric Properties of $Pb[Zr_{0.45}Ti_{0.5-x}Lu_x(Mn_{1/3}Sb_{2/3})_{0.05}]O_3$ Ceramics," *Journal of the American Ceramic Society,* vol. 81, pp. 2473-2476, 1998.

[11] E. Koray Akdogan, M. Allahverdi, and A. Safari, "Piezoelectric composites for sensor and actuator applications," *Ultrasonics, Ferroelectrics and Frequency Control, IEEE Transactions on,* vol. 52, pp. 746-775, 2005.

[12] R. C. Pullar, Y. Zhang, L. Chen, S. Yang, J. R. Evans, P. K. Petrov, A. N. Salak, D. A. Kiselev, A. L. Kholkin, and V. M. Ferreira, "Manufacture and measurement of combinatorial libraries of dielectric ceramics: Part II. Dielectric measurements of $Ba_{1-x}Sr_xTiO_3$ libraries," *Journal of the European Ceramic Society,* vol. 27, pp. 4437-4443, 2007.

[13] *Piezoelectric Ceramics: Principles and Applications*: APC International Ltd., 2011.

[14] S.-E. Park and T. R. Shrout, "Ultrahigh strain and piezoelectric behavior in relaxor based ferroelectric single crystals," *Journal of Applied Physics,* vol. 82, pp. 1804-1811, 1997.

[15] S.-E. Park and T. R. Shrout, "Characteristics of relaxor-based piezoelectric single crystals for ultrasonic transducers," *Ultrasonics, Ferroelectrics and Frequency Control, IEEE Transactions on,* vol. 44, pp. 1140-1147, 1997.

[16] E. Fukada, "History and recent progress in piezoelectric polymers," *Ultrasonics, Ferroelectrics and Frequency Control, IEEE Transactions on,* vol. 47, pp. 1277-1290, 2000.

[17] H. Gallantree, "Piezoelectric ceramic/polymer composites," in *Br. Ceram. Proc.*, 1987, pp. 161-169.

[18] N. Emanetoglu, C. Gorla, Y. Liu, S. Liang, and Y. Lu, "Epitaxial ZnO piezoelectric thin films for saw filters," *Materials Science in Semiconductor Processing,* vol. 2, pp. 247-252, 1999.

[19] P. Muralt, R. Polcawich, and S. Trolier-McKinstry, "Piezoelectric thin films for sensors, actuators, and energy harvesting," *MRS bulletin,* vol. 34, pp. 658-664, 2009.
[20] T. R. Shrout and S. J. Zhang, "Lead-free piezoelectric ceramics: Alternatives for PZT?," *Journal of Electroceramics,* vol. 19, pp. 113-126, 2007.
[21] A. Moulson and J. Herbert, "Piezoelectric ceramics," *Electroceramics: Materials, Properties, Applications, Second Edition,* pp. 339-410, 2003.
[22] D. Berlincourt, "Piezoelectric crystals and ceramics," in *Ultrasonic Transducer Materials*, ed: Springer, 1971, pp. 63-124.
[23] H. JAFFE, "Piezoelectric ceramics," *Journal of the American Ceramic Society,* vol. 41, pp. 494-498, 1958.
[24] L. Egerton and D. M. Dillon, "Piezoelectric and dielectric properties of ceramics in the system potassium—sodium niobate," *Journal of the American Ceramic Society,* vol. 42, pp. 438-442, 1959.
[25] Y. Guo, K.-i. Kakimoto, and H. Ohsato, "$(Na_{0.5}K_{0.5})NbO_3$–$LiTaO_3$ lead-free piezoelectric ceramics," *Materials Letters,* vol. 59, pp. 241-244, 2005.
[26] R. Smith and F. Welsh, "Temperature dependence of the elastic, piezoelectric, and dielectric constants of lithium tantalate and lithium niobate," *Journal of applied physics,* vol. 42, pp. 2219-2230, 1971.
[27] H. Jaffe and D. A. Berlincourt, "Piezoelectric transducer materials," *Proceedings of the IEEE,* vol. 53, pp. 1372-1386, 1965.
[28] Y. Xu, "Ferroelectric materials and their applications," 1991.
[29] R. Rai, S. Sharma, and R. Choudhary, "Dielectric and piezoelectric studies of Fe doped PLZT ceramics," *Materials Letters,* vol. 59, pp. 3921-3925, 2005.
[30] N. K. James, D. van den Ende, U. Lafont, S. van der Zwaag, and W. A. Groen, "Piezoelectric and mechanical properties of structured PZT–epoxy composites," *Journal of Materials Research,* vol. 28, pp. 635-641, 2013.
[31] V. Janicek and M. Husak, "Polymer based Piezoelectric Energy Microgenerator," in *International Conference of Renewable Energies and Power Quality*, 2010, p. 528.
[32] R. Bechmann, "Elastic and piezoelectric constants of alpha-quartz," *Physical review,* vol. 110, p. 1060, 1958.
[33] J. G. Webster and H. Eren, *Measurement, Instrumentation, and Sensors Handbook: Spatial, Mechanical, Thermal, and Radiation Measurement* vol. 1: CRC press, 2014.
[34] E. Cross, "Materials science: Lead-free at last," *Nature,* vol. 432, pp. 24-25, 2004.
[35] B. Noheda, J. Gonzalo, L. Cross, R. Guo, S.-E. Park, D. Cox, and G. Shirane, "Tetragonal-to-monoclinic phase transition in a ferroelectric perovskite: the structure of $PbZr_{0.52}Ti_{0.48}O_3$," *Physical Review B,* vol. 61, p. 8687, 2000.
[36] D. Damjanovic, "A morphotropic phase boundary system based on polarization rotation and polarization extension," *Applied Physics Letters,* vol. 97, p. 062906, 2010.
[37] A. Pramanick, A. D. Prewitt, M. A. Cottrell, W. Lee, A. J. Studer, K. An, C. R. Hubbard, and J. L. Jones, "In situ neutron diffraction studies of a commercial, soft lead zirconate titanate ceramic: response to electric fields and mechanical stress," *Applied Physics A,* vol. 99, pp. 557-564, 2010.
[38] G. H. Haertling, "Ferroelectric ceramics: history and technology," *Journal of the American Ceramic Society,* vol. 82, pp. 797-818, 1999.

[39] A. Safari, "Development of piezoelectric composites for transducers," *Journal de Physique III,* vol. 4, pp. 1129-1149, 1994.

[40] R. Newnham, D. Skinner, and L. Cross, "Connectivity and piezoelectric-pyroelectric composites," *Materials Research Bulletin,* vol. 13, pp. 525-536, 1978.

[41] D. van den Ende, *Structured Piezoelectric Composites: Materials and Applications*: Doctoral Thesis, 2012.

[42] R. Newnham, A. Safari, J. Giniewicz, and B. Fox, "Composite piezoelectric sensors," *Ferroelectrics,* vol. 60, pp. 15-21, 1984.

[43] D. Van den Ende, B. Bory, W. Groen, and S. Van der Zwaag, "Improving the d_{33} and g_{33} properties of 0-3 piezoelectric composites by dielectrophoresis," *Journal of Applied Physics,* vol. 107, p. 024107, 2010.

[44] G. Sa-Gong, A. Safari, S. Jang, and R. Newnham, "Poling flexible piezoelectric composites," *Ferroelectrics Letters Section,* vol. 5, pp. 131-142, 1986.

[45] B. Satish, K. Sridevi, and M. Vijaya, "Study of piezoelectric and dielectric properties of ferroelectric PZT-polymer composites prepared by hot-press technique," *Journal of Physics D: Applied Physics,* vol. 35, p. 2048, 2002.

[46] W. Sakamoto, P. Marin-Franch, and D. Das-Gupta, "Characterization and application of PZT/PU and graphite doped PZT/PU composite," *Sensors and Actuators A: Physical,* vol. 100, pp. 165-174, 2002.

[47] T. Yamada, T. Ueda, and T. Kitayama, "Piezoelectricity of a high-content lead zirconate titanate/polymer composite," *Journal of Applied Physics,* vol. 53, pp. 4328-4332, 1982.

[48] I. Babu, D. Van Den Ende and and G. de With, "Processing and characterization of piezoelectric 0-3 PZT/LCT/PA composites," *Journal of Physics D: Applied Physics,* vol. 43, p. 425402, 2010.

[49] D. Van den Ende, P. De Almeida, and S. Van der Zwaag, "Piezoelectric and mechanical properties of novel composites of PZT and a liquid crystalline thermosetting resin," *Journal of materials science,* vol. 42, pp. 6417-6425, 2007.

[50] N. James, U. Lafont, S. van der Zwaag, and W. Groen, "Piezoelectric and mechanical properties of fatigue resistant, self-healing PZT–ionomer composites," *Smart Materials and Structures,* vol. 23, p. 055001, 2014.

[51] K.-h. Lam, W. XIAOXING, and H. L.-w. Chan, "Piezoelectric and pyroelectric properties of $(Bi_{0.5}Na_{0.5})0.94\ Ba_{0.06}TiO_3$/P(VDF-TrFE) 0-3 composites," *Composites. Part A, Applied science and manufacturing,* vol. 36, pp. 1595-1599, 2005.

[52] I. R. Abothu, S.-F. Liu, S. Komarneni, and Q. H. Li, "Processing of Pb $(Zr_{0.52}Ti_{0.48})O_3$ (PZT) ceramics from microwave and conventional hydrothermal powders," *Materials research bulletin,* vol. 34, pp. 1411-1419, 1999.

[53] W. Wersing, W. Rossner, G. Eckstein, and G. Tomandl, "The morphotropic phase boundary in PZT ceramics prepared by spray, drying of salt solutions and by the mixed oxide method," *Silicates industriels,* vol. 50, pp. 41-46, 1985.

[54] A. Trogé, R. L. O'Leary, G. Hayward, R. A. Pethrick, and A. J. Mullholland, "Properties of photocured epoxy resin materials for application in piezoelectric ultrasonic transducer matching layers," *The Journal of the Acoustical Society of America,* vol. 128, pp. 2704-2714, 2010.

[55] M. Ivankovic, I. Brnardic, H. Ivankovic, and H. J. Mencer, "DSC study of the cure kinetics during nanocomposite formation: epoxy/poly (oxypropylene) diamine/organically modified montmorillonite system," *Journal of applied polymer science,* vol. 99, pp. 550-557, 2006.

[56] J. Tressler, S. Alkoy, A. Dogan, and R. Newnham, "Functional composites for sensors, actuators and transducers," *Composites Part A: Applied Science and Manufacturing,* vol. 30, pp. 477-482, 1999.

[57] M. C. Araújo, C. Costa, and S. Lanceros-Méndez, "Evaluation of dielectric models for ceramic/polymer composites: Effect of filler size and concentration," *Journal of Non-Crystalline Solids,* vol. 387, pp. 6-15, 2014.

[58] C. Dias and D. Das-Gupta, "Inorganic ceramic/polymer ferroelectric composite electrets," *Dielectrics and Electrical Insulation, IEEE Transactions on,* vol. 3, pp. 706-734, 1996.

[59] R. Newnham, "Ferroelectric composites," *Japanese Journal of Applied Physics,* vol. 24, p. 16, 1985.

[60] C. Bowen and V. Y. Topolov, "Piezoelectric sensitivity of $PbTiO_3$-based ceramic/polymer composites with 0–3 and 3–3 connectivity," *Acta materialia,* vol. 51, pp. 4965-4976, 2003.

[61] J. Sheen, Z.-W. Hong, C.-W. Su, and H.-C. Chen, "Microwave measurements of dielectric constants by exponential and logarithmic mixture equations," *Progress In Electromagnetics Research,* vol. 100, pp. 13-26, 2010.

[62] T. Furukawa, K. Ishida, and E. Fukada, "Piezoelectric properties in the composite systems of polymers and PZT ceramics," *Journal of Applied Physics,* vol. 50, pp. 4904-4912, 1979.

[63] K. Wagner, "Erklärung der dielektrischen Nachwirkungsvorgänge auf Grund Maxwellscher Vorstellungen," *Archiv für Elektrotechnik,* vol. 2, pp. 371-387, 1914/09/01 1914.

[64] S.-D. Cho, S.-Y. Lee, J.-G. Hyun, and K.-W. Paik, "Comparison of theoretical predictions and experimental values of the dielectric constant of epoxy/$BaTiO_3$ composite embedded capacitor films," *Journal of Materials Science: Materials in Electronics,* vol. 16, pp. 77-84, 2005.

[65] N. Jayasundere and B. Smith, "Dielectric constant for binary piezoelectric 0-3 composites," *Journal of Applied Physics,* vol. 73, pp. 2462-2466, 1993.

[66] A. Goncharenko, V. Lozovski, and E. Venger, "Lichtenecker's equation: applicability and limitations," *Optics Communications,* vol. 174, pp. 19-32, 2000.

[67] R. Simpkin, "Derivation of Lichtenecker's logarithmic mixture formula from Maxwell's equations," *Microwave Theory and Techniques, IEEE Transactions on,* vol. 58, pp. 545-550, 2010.

[68] N. Maron and O. Maron, "Criteria for mixing rules application for inhomogeneous astrophysical grains," *Monthly Notices of the Royal Astronomical Society,* vol. 391, pp. 738-764, 2008.

[69] T. Furukawa, K. Fujino, and E. Fukada, "Electromechanical properties in the composites of epoxy resin and PZT ceramics," *Japanese Journal of Applied Physics,* vol. 15, p. 2119, 1976.

[70] E. Venkatragavaraj, B. Satish, P. Vinod, and M. Vijaya, "Piezoelectric properties of ferroelectric PZT-polymer composites," *Journal of Physics D: Applied Physics,* vol. 34, p. 487, 2001.

[71] M. T. Sebastian and H. Jantunen, "Polymer–ceramic composites of 0–3 connectivity for circuits in electronics: a review," *International Journal of Applied Ceramic Technology,* vol. 7, pp. 415-434, 2010.

[72] H. T. Vo and F. G. Shi, "Towards model-based engineering of optoelectronic packaging materials: Dielectric constant modeling," *Microelectronics Journal,* vol. 33, pp. 409-415, 2002.

[73] N. Jayasundere, B. Smith, and J. Dunn, "Piezoelectric constant for binary piezoelectric 0-3 connectivity composites and the effect of mixed connectivity," *Journal of applied physics,* vol. 76, pp. 2993-2998, 1994.

[74] A. Boutarfaia, "Investigations of co-existence region in lead zirconate-titanate solid solutions: X-ray diffraction studies," *Ceramics International,* vol. 26, pp. 583-587, 2000.

[75] A. Boutarfaia, "Study of the solid state reaction and the morphotropic phase boundary in $Pb(Zr,Ti)O_3$-$Pb(Fe_{1/5},Ni_{1/5},Sb_{3/5})O_3$ ceramics," *Ceramics International,* vol. 27, pp. 91-97, 2001.

[76] A. Boutarfaia, C. Boudaren, A. Mousser, and S. Bouaoud, "Study of phase transition line of PZT ceramics by X-ray diffraction," *Ceramics international,* vol. 21, pp. 391-394, 1995.

[77] S. Fushimi and T. Ikeda, "Phase Equilibrium in the System PbO-TiO_2–ZrO_2," *Journal of the American Ceramic Society,* vol. 50, pp. 129-132, 1967.

[78] Z. Li and H. Gonga, "Effects of particle size on the piezoelectric properties of 0–3 PZT/cement composites," in *MULTISCALE AND FUNCTIONALLY GRADED MATERIALS 2006:(M&FGM 2006)*, 2008, pp. 538-543.

[79] C. A. Randall, N. Kim, J. P. Kucera, W. Cao, and T. R. Shrout, "Intrinsic and Extrinsic Size Effects in Fine-Grained Morphotropic-Phase-Boundary Lead Zirconate Titanate Ceramics," *Journal of the American Ceramic Society,* vol. 81, pp. 677-688, 1998.

[80] H. Martirena and J. Burfoot, "Grain-size effects on properties of some ferroelectric ceramics," *Journal of Physics C: Solid State Physics,* vol. 7, p. 3182, 1974.

[81] A. Safari and E. K. Akdogan, *Piezoelectric and acoustic materials for transducer applications*: Springer, 2008.

[82] N. Vittayakorn, G. Rujijanagul, T. Tunkasiri, X. Tan, and D. P. Cann, "Perovskite phase formation and ferroelectric properties of the lead nickel niobate–lead zinc niobate–lead zirconate titanate ternary system," *Journal of materials research,* vol. 18, pp. 2882-2889, 2003.

[83] D. S. Lee, C. W. Ahn, I. W. Kim, H. Y. Choi, Y. H. Jeong, J. S. Lee, J. S. Song, B. K. Min, and S. J. Jeong, "The sintering behavior and piezoelectric properties of $Pb(Ni_{1/3}Nb_{2/3})O_3$-$PbTiO_3$-$PbZrO_3$ ceramics using two-step calcination," 2003.

[84] A. Prasatkhetragarn, N. Triamnak, R. Yimnirun, and D. Cann, "Morphotropic Phase Boundary of $0.875Pb(Zr_xTi_{1-x})O_3$–$0.125Pb(Mg_{1/3}Nb_{2/3})O_3$ Ceramics," *Ferroelectrics,* vol. 470, pp. 280-286, 2014.

[85] K. H. Yoon and H. R. Lee, "Electric-field-induced strain and piezoelectric properties near the morphotropic phase boundary of $Pb(Mg_{1/3}Nb_{2/3})O_3$–$PbZrO_3$–$PbTiO_3$ ceramics," *Journal of Applied Physics,* vol. 89, pp. 3915-3919, 2001.

[86] Y. Cao, G. Sheng, J. X. Zhang, S. Choudhury, Y. L. Li, C. A. Randall, and L. Q. Chen, "Piezoelectric response of single-crystal $PbZr_{1-x}Ti_xO_3$ near morphotropic phase boundary predicted by phase-field simulation," *Applied Physics Letters,* vol. 97, pp. -, 2010.
[87] R. Waser, *Nanoelectronics and information technology*: John Wiley & Sons, 2012.
[88] M.-C. Wang, M.-S. Huang, T.-S. Wong, and N.-C. Wu, "Sintering and piezoelectric properties of $Pb(Ni_{1/3}Sb_{2/3})O_3$-$PbZrO_3$-$PbTiO_3$ ceramics," *Journal of Materials Science,* vol. 37, pp. 663-668, 2002/02/01 2002.
[89] B. Chambion, L. Goujon, L. Badie, Y. Mugnier, C. Barthod, C. Galez, S. Wiebel, and C. Venet, "Optimization of the piezoelectric response of 0–3 composites: a modeling approach," *Smart Materials and Structures,* vol. 20, p. 115006, 2011.
[90] H. Khanbareh, S. van der Zwaag, and W. Groen, "Effect of dielectrophoretic structuring on piezoelectric and pyroelectric properties of lead titanate-epoxy composites," *Smart Materials and Structures,* vol. 23, p. 105030, 2014.
[91] M. Taya, *Electronic composites: modeling, characterization, processing, and MEMS applications*: Cambridge University Press, 2005.